The Physics of Fluids

Review Article: Nonlinear mode conversion and anomalous absorption processes during radio-frequency heating of bumpy torus plasmas

by V. Stefan and N. A. Krall

Volume 28 October 1985 Number 10

a publication of the American Institute of Physics

Nonlinear mode conversion and anomalous absorption processes during radio-frequency heating of bumpy torus plasmas

V. Stefan and N. A. Krall
JAYCOR, P. O. Box 85154, San Diego, California 92138

(Received 17 December 1984; accepted 18 June 1985)

The theory of nonlinear mode conversion is reviewed and applied to the ELMO Bumpy Torus (EBT) [*Proceedings of the 5th International Conference on Plasma Physics and Controlled Nuclear Fusion Research 1974* (IAEA, Vienna, 1975), Vol. 2, p. 141] environment in the electron-cyclotron, upper-hybrid, lower-hybrid, and ion-cyclotron frequency ranges. A variety of parametric excitations in these frequency ranges is studied. Based on cascade saturation mechanisms, the parametric turbulence levels and corresponding anomalous absorption rates of the excited modes are evaluated. The relevance of nonlinear mode conversion for contemporary and future EBT experiments is discussed.

I. INTRODUCTION

The aim of this study is to present a theory of nonlinear mode conversion and anomalous plasma heating that can take place in ELMO Bumpy Torus (EBT)[1] experiments. Four frequency domains are considered: electron-cyclotron (EC), upper-hybrid (UH), lower-hybrid (LH), and ion-cyclotron (IC) frequencies. The primary motivation for the study is to evaluate the significance of parametric processes in electromagnetic (EM) wave–EBT plasma interactions[2] and, more specifically, in wave heating of EBT plasma. Further, the calculations given in what follows could also be used in investigating the possibility of "nonlinear control" in EBT, e.g., new ways of production of *e*- and *i*-rings, their location, modification of startup conditions, etc. Lastly, the procedure used in this review could be formally directly applied to other similar plasma configurations, e.g., mirrors.

In the EBT fusion scheme,[1] as it stands now, waves in the electron cyclotron frequency range (ECFR) play a crucial role. They are used in steady-state plasma creation, in plasma sustainment, and in core plasma heating. In addition, wave absorption in the second electron-cyclotron harmonic resonance layer plays a dominant role in the production of the hot electron annulus[3] required for stability.

Plasma heating in this frequency range is made possible by recent[4] encouraging development of gyrotrons. Further, accessibility of EC waves in the high plasma density regions of fusion devices is more effective when compared to, for example, the LH and/or IC frequency range. In a tokamak, this frequency range has been relatively well-explored experimentally[5] and theoretically in the framework of linear theory.[6] A similar situation exists in mirror plasma configurations where ECFR has been utilized for bulk plasma heating in a central cell of tandem mirrors and for generation of energetic electrons in a single-cell mirror or in the end plugs of tandem mirrors.[7]

Theoretical studies of heating in EBT have been based largely on linear absorption models, leading to a qualitative understanding of the core heating. For this complicated, asymmetrical geometry, ray tracing must be used to determine details of wave propagation. A central feature is the extraordinary mode right-hand cutoff, which prevents the X mode injected into the mirror midplane from directly reaching the fundamental resonant zone in the mirror throat. This is significant because for typical core conditions, ordinary mode direct absorption is negligible both at the fundamental and at the second harmonic resonance, while heating by the X mode at the second harmonic is similarly small. Nevertheless, the core is observed to be strongly heated, testifying to the fact that either the X mode is reaching the fundamental resonance, or a nonlinear process is allowing either strong absorption of X modes at the second harmonic surface or strong absorption of the O mode at either fundamental or second harmonic. These are the processes investigated in the ECFR portions of this review.

A similar situation occurs for the lower frequency ranges (lower hybrid through ion cyclotron). Experiments over a variety of frequency ranges show ion heating increasing with frequency when the frequency was above an onset frequency that allows wave propagation. Both experimentally and theoretically this onset frequency is of order 30 MHz for density $n \simeq 10^{12}$ cm^{-3} and $B \sim 5.5$ kG. The heating observed in EBT-S for a wave frequency of 30 MHz is substantial. The mechanism by which the ions are heated is unlikely to be linear wave absorption, since simplified theoretical models predict only weak absorption by linear ion-cyclotron wave damping for EBT-S parameters. Both the increase in ion energy density and the short decay times when the ion wave source is switched off attest to anomalously strong absorption from ICRH fields. Various nonlinear mechanisms have been proposed to explain the discrepancy, including coupling of fast and slow wave fields by plasma inhomogeneities, mode conversion processes, and production of lower-hybrid fluctuations through an oscillating two-stream instability at ion-cyclotron harmonics. All of these processes could contribute in various parameter ranges. The lower-frequency portion of this review concentrates on parametric absorption processes, which should come into play as the ion-cyclotron frequency range (ICFR) power increases.

 0031-9171/85/102937-23$01.90

For a reactor size EBT, gyrotrons capable of generating more than 1 MW of power in a continuous wave (CW) mode of operation will be required. At present, 200 kW tubes are available in CW operation (pulse duration $\tau \gtrsim 10$ msec), and around 1 MW in pulsed operation ($\tau \sim 100\,\mu$sec). These high power levels suggest that nonlinear processes could already play a significant role in EBT plasma heating and *e*- or *i*-ring production,[8] and we here investigate that suggestion.

Although the electron-cyclotron frequency range has been basic in the electromagnetic wave–EBT plasma interaction,[8–10] from the beginning of research in EBT other frequency domains have been (relatively less) studied. Recently, lower-hybrid frequency range (LHFR)[11] and ion-cyclotron frequency range (ICFR)[12,13] waves have attracted significant attention both for the heating of core plasma and possibly for the production of an ion annulus.[14] However, the foundations of rf plasma heating theory in LHFR and ICFR are presently largely based on tokamak applications, both for linear and nonlinear theory (see, for example, Ref. 15 and references therein). Here we extend and modify these foundations as appropriate for EBT applications.

The organization of this review is as follows. In Sec. II we give the relevant aspects of nonlinear mode conversion theory for a range of parameters typical of EBT experiments in the electron-cyclotron, lower-hybrid, and ion-cyclotron frequency domains. We present a parametric excitation theory including plasma inhomogeneity, finite extent of the driver pump, and driver pump finite wavelength. We also take into account convection of the excited electrostatic modes in various frequency ranges. Accordingly, the treatment of thresholds and growth rates is given in a unified manner. The problem of identifying the convective or absolute character of the instabilities is beyond the scope of this review because it demands a self-consistent treatment of driver pump propagation and plasma response in the resonance layers. However, in some cases, such identification has already been stated in the literature; we use any such available material in our calculations. In the frame of weak parametric turbulence theory, cascading saturation mechanisms are involved, being the most effective saturation mechanisms for the frequency mismatches considered in this work. In the lower-hybrid frequency we also discuss the relevance of strong parametric turbulence processes based on rate equations. In Secs. III and IV, threshold values, parametric growth rates, turbulence levels, and nonlinearly absorbed energy in electron-cyclotron and upper-hybrid resonances are given. Section V deals with nonlinear processes at the edge and interior of an EBT plasma, considering excitation of Gould–Trivelpiece modes and lower-hybrid waves. In Sec. VI we study nonlinear processes at ion-cyclotron harmonic resonances. Limitations of the validity of the theory and possibilities of observing nonlinear effects in contemporary and future EBT experiments are discussed in Sec. VII.

II. NEAR-THRESHOLD NONLINEAR MODE CONVERSION THEORY

This section will be dedicated to a general presentation of the nonlinear mode conversion theory, emphasizing those aspects that are specific for EM wave–EBT plasma interaction. In other words, the case of weak driver pumps when spatial amplification length of excited high-frequency waves is larger than the spatial damping length of low-frequency modes is considered.

A. Parametric excitation

Consider the interaction of X- and O-mode driver pumps with the electric field $\mathbf{E}(\mathbf{r},t) = \mathbf{E}_0 \sin(\omega_0 t - \mathbf{k}_0 \cdot \mathbf{r})$ with a low-β inhomogeneous plasma (for EBT-S, $\beta \sim 6\times 10^{-3}$). The relevant inhomogeneity gradients are oriented along the x and y axis (see Fig. 1). In the linear phase of the development of decay parametric instabilities, the evolution of the excited oscillations in $(\omega,\mathbf{k})$ space is governed by the weak mode–mode coupling dispersion relation given by[16,17]

$$\epsilon(\omega + i\gamma,\mathbf{k})\epsilon(\omega - \omega_0 + i\gamma,\mathbf{k} - \mathbf{k}_0) + \mu^2 = 0. \tag{1}$$

Here $\epsilon(\omega + i\gamma,\mathbf{k}) \equiv \epsilon_L$ and $\epsilon(\omega - \omega_0 + i\gamma,\mathbf{k} - \mathbf{k}_0) \equiv \epsilon_H$ are the low- and high-frequency plasma dielectric permittivities[18,19] (see Appendix A), respectively, μ is the wave coupling coefficient, and γ is the parametric growth rate. Equation (1) describes parametric decay processes, i.e., three-wave interaction process of a driver pump with a Stokes' sideband at $(\omega - \omega_0, \mathbf{k} - \mathbf{k}_0)$ and a beat wave at $(\omega,\mathbf{k})$. By Taylor expansion of the mode–mode coupling dispersion relation (1) in ω space we obtain

$$(\gamma + \gamma_H)(\gamma + \gamma_L) + \mu^2 \left(\frac{\partial\, \mathrm{Re}\,\epsilon_H}{\partial\omega}\right)^{-1}_{\omega=\omega_H} \left(\frac{\partial\, \mathrm{Re}\,\epsilon_L}{\partial\omega}\right)^{-1}_{\omega=\omega_L} = 0, \tag{2}$$

where γ_H, γ_L are the linear damping rates of high- and low-frequency modes, respectively, and Re denotes real part. The nonlinear mode coupling relation (2) describes formally two kinds of parametric excitations. First is the excitation of high-frequency modes coupled to low-frequency modes with appropriate coupling coefficients. In the electron-cyclotron frequency range (ECFR), we shall study excitation of electron-cyclotron (EC) and upper-hybrid (UH) waves, as high-frequency modes, coupled to ion-acoustic, lower-hybrid,

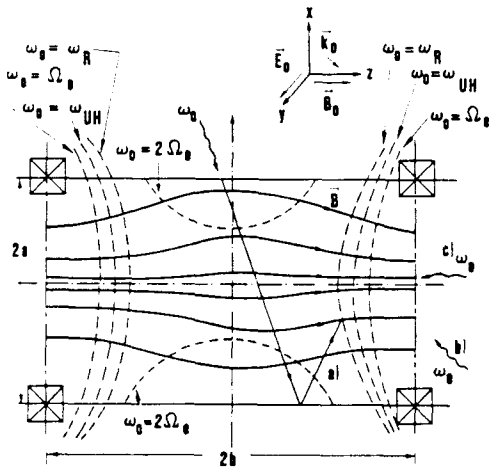

FIG. 1. Magnetic field and electromagnetic wave geometry in one mirror cell are shown. Case (a) denotes a reflected wave from the wall and (b) and (c) a reflected wave in the next mirror cell and high-field launching, respectively. The length is 2b; 2a is the width of one mirror section.

and ion-cyclotron waves, as low-frequency modes. In the lower-hybrid frequency range we study coupling of lower-hybrid and Gould–Trivelpiece waves with ion-cyclotron and ion-Bernstein waves. In the ion-cyclotron frequency range we study excitation of ion-cyclotron harmonics by a magnetosonic wave pump.

With appropriately evaluated coupling coefficients, relation (2) describes, also, excitation of two modes of the same nature (for example, two electron-cyclotron, lower-hybrid, or ion-cyclotron waves). In this case, in (1) and (2) $\gamma_L \equiv \gamma_H$ and $\epsilon_L \equiv \epsilon_H$. Frequencies and wave vectors of the external driver pump $(\omega_0, \mathbf{k}_0)$ and the excited wave $(\omega_L, \mathbf{k}_L)$, $(\omega_L - \omega_0, \mathbf{k}_L - \mathbf{k}_0)$ satisfy the following selection rules: $\omega_0(\mathbf{k}_0) = \omega_L(\mathbf{k}_L) + \omega_H(\mathbf{k}_H)$,$(\omega_H \equiv \omega_L - \omega_0, \quad \mathbf{k}_H \equiv \mathbf{k}_L - \mathbf{k}_0)$, and $\mathbf{k}_0 = \mathbf{k}_L + \mathbf{k}_H$.

The linear phase of the development of parametric instabilities is extensively studied in Refs. 16, 17, and 20. Based on the Vlasov–Poisson formalism of parametric instabilities of longitudinal waves in magnetized plasma, we obtain for the threshold value of the wave coupling coefficient, in the case of excitation of the low-frequency mode,

$$(\mu_L^T)^2 \equiv \frac{k^2 \operatorname{Re}\chi_i(\omega,\mathbf{k})[1+\operatorname{Re}\chi_e(\omega,\mathbf{k})]}{4}\left(\frac{eE_0^T}{m_e\omega_0^2}\right)^2 f(\theta,\zeta,\chi)$$

$$= \left(\frac{\partial \operatorname{Re}\epsilon_H}{\partial\omega}\right)_{\omega=\omega_H}\left(\frac{\partial \operatorname{Re}\epsilon_L}{\partial\omega}\right)_{\omega=\omega_L} A_1, \tag{3}$$

where A_1 specifies the dissipative, convective, and inhomogeneous electric field thresholds, respectively,

$$A_1 = \gamma_H\gamma_L = \frac{(\gamma_H V_L + \gamma_L V_H)^2}{4V_H V_L} = \frac{V_H V_L}{L_M^2}. \tag{4}$$

In (4), L_M is the length corresponding to mismatching of wave vectors caused by the plasma inhomogeneity. It is given by $L_M = (2\pi/|\partial\Delta k_i/\partial i|)^{1/2}$, with $\Delta k_i = k_{0i} - k_{Li} - k_{Hi}$, where i denotes the axis along the relevant inhomogeneity gradient.

The dissipative threshold is obtained from Eq. (2) by setting $\gamma = 0$, and gives the intensity of the electric field required to cancel the linear dissipation (collisional or noncollisional) of the excited modes. The convective threshold is obtained from a model of homogeneous plasma that takes into account the convective character of the excited waves (for a mathematical treatment, see Refs. 19 and 21). The threshold caused by the plasma inhomogeneity is a well-known result of Rosenbluth.[22] In our presentation it is directly obtained from Eq. (2) ($\gamma = 0$), introducing equivalent dissipation of excited modes $\gamma_H \to V_H/L_M$ and $\gamma_L \to V_L/L_M$, where γ_H, V_H and γ_L, V_L are the linear damping rates and group velocities of high- and low-frequency modes, respectively.

The threshold caused by the finite extent of the pump is obtained from the third term in (4) by putting $L_M \to L$, where L is the effective extent of the driver pump. In EBT experiments this threshold is lower ($L > L_M$) than the inhomogeneous one. In (3), E_0^T is the threshold value of the driver pump electric field, $\operatorname{Re}\chi_i(\omega,\mathbf{k})$ and $\operatorname{Re}\chi_e(\omega,\mathbf{k})$ are the real parts of the low-frequency ion and electron linear plasma susceptibilities, and e, m_e are the electron charge and mass, respectively.

The function $f(\theta,\zeta,\chi)$ describes the geometry of the interaction and has the form:

$$f(\theta,\zeta,\chi) = \left[\cos\theta\cos\chi + \left(\frac{\omega_0^2}{\omega_0^2-\Omega_e^2} - \frac{\omega_0^2}{\omega_0^2-\Omega_i^2}\right)\sin\theta\sin\chi\cos\zeta\right]^2 + \left[\sin\theta\sin\chi\sin\zeta\left(\frac{\omega_0\Omega_e}{\omega_0^2-\Omega_e^2} - \frac{\omega_0\Omega_i}{\omega_0^2-\Omega_i^2}\right)\right]^2. \tag{5}$$

Here θ is the angle between the vectors $(\mathbf{k} - \mathbf{k}_0)$ and $\mathbf{B}_0$, χ is the angle between $\mathbf{B}_0$ and $\mathbf{E}_0$, and ζ is the angle between two planes formed by two pairs of vectors, $(\mathbf{k} - \mathbf{k}_0, \mathbf{B}_0)$ and $(\mathbf{B}_0, \mathbf{E}_0)$.

The coupling coefficient (3) can be written in somewhat different form:

$$\mu_L^2 = \frac{k^2|(\mathbf{k}-\mathbf{k}_0)\cdot\mathbf{r}_{EB}|^2}{4(\mathbf{k}-\mathbf{k}_0)^2}\operatorname{Re}\chi_i(\omega,\mathbf{k})[1+\operatorname{Re}\chi_e(\omega,\mathbf{k})], \tag{6}$$

where $\mathbf{r}_{EB}$ is the amplitude of the complex vector describing the oscillation of electrons with respect to the ions in the driver pump electric field $\mathbf{E}_0$ and the dc magnetic field $\mathbf{B}_0$, and is given by

$$\mathbf{r}_{EB} = E_{0x}\left(\frac{e}{m_e}\frac{1}{\omega_0^2-\Omega_e^2} - \frac{e_i}{m_i}\frac{1}{\omega_0^2-\Omega_i^2}\right) - iE_{0y}\left(\frac{e}{m_e}\frac{\Omega_e}{\omega_0(\omega_0^2-\Omega_e^2)} - \frac{e_i}{m_i}\frac{\Omega_i}{\omega_0(\omega_0^2-\Omega_i^2)}\right)$$

$$= iE_{0x}\left(\frac{e}{m_e}\frac{\Omega_e}{\omega_0(\omega_0^2-\Omega_e^2)} - \frac{e_i}{m_i}\frac{\Omega_i}{\omega_0(\omega_0^2-\Omega_i^2)}\right) + E_{0y}\left(\frac{e}{m_e}\frac{1}{\omega_0^2-\Omega_e^2} - \frac{e_i}{m_i}\frac{1}{\omega_0^2-\Omega_i^2}\right)$$

$$= E_{0z}\left(\frac{e}{m_e\omega_0^2} - \frac{e_i}{m_i\omega_0^2}\right). \tag{7}$$

In (6), $\chi_i(\omega,\mathbf{k})$ and $\chi_e(\omega,\mathbf{k})$ are the linear ion and electron susceptibilities at low frequency, respectively, and $\mathbf{k}$ is the wave vector of the low-frequency (beat) mode. In (7), Ω_e and Ω_i are the electron and ion-cyclotron frequencies, respectively.

If two modes with approximately the same frequencies are excited, the coupling coefficient takes the form

$$(\mu_H^T)^2 \equiv \frac{(\mathbf{k}_0, 2\mathbf{k}-\mathbf{k}_0)^2}{k^2}\left(\frac{eE_0^T}{m_e\omega_0^2}\right)^2 f(\theta,\xi,\chi)$$

$$= \left(\frac{\partial \operatorname{Re}\epsilon_H}{\partial\omega}\right)_{\omega=\omega_H} A_2, \tag{8}$$

where $A_2 \equiv A_1$ for $V_L \to V_H$ and $\gamma_L \to \gamma_H$. In somewhat different form (8) reads

$$\mu_H^2 = \frac{|(\mathbf{k}-\mathbf{k}_0)\cdot\mathbf{r}_{EB}|^2}{k^2(\mathbf{k}-\mathbf{k}_0)^2}(2\mathbf{k}\cdot\mathbf{k}_0 - \mathbf{k}_0^2)^2. \tag{9}$$

We note that a weak coupling approximation in the parametric dispersion relation [see (1) and (2)] is employed because of the relatively low driver pump electric field intensities available per mirror section in contemporary EBT experiments.

As seen from (3) and (4), the threshold value for convective instability [first term in (4)] is lower in the homogeneous plasma, in general, than the threshold value for absolute instabilities [second term in (4)]. In inhomogeneous plasma it was shown in Ref. 22 that, once threshold value [third term in (4)] has been exceeded, parametric instabilities will evolve as convective. More subtle treatment of the problem to include spatial structure[23] of the driver pump electric field caused by the plasma inhomogeneity, shows that parametric instabilities can evolve as convective or absolute depending on plasma parameters and wavenumbers of the excited waves. The problem of establishing the character of parametric instabilities is beyond the scope of this review and in the following anomalous absorption will be treated for convective instabilities as more likely to appear in the presence of the weak driver pump electric field. The influence of a convective and/or absolute character of parametric instabilities on anomalous absorption in relatively stronger driver pump electric fields (more typical for tokamaks) was addressed in Refs. 24 and 25. In the case of excitation of convective parametric instabilities, relevant quantities are the spatial growth rate Im k and spatial linear damping rates Im k_H, Im k_L of high- and low-frequency modes, respectively. By Taylor expansion of the mode–mode coupling dispersion relation[16] in k space, we obtain

$$\left(\operatorname{Im} k_i + \frac{\gamma_H}{V_{H,i}}\right)\left(\operatorname{Im} k_i + \frac{\gamma_L}{V_{L,i}}\right) = \frac{\gamma_{d0}^2}{|V_{H,i}V_{L,i}|}, \tag{10}$$

where

$$\gamma_{d0}^2 = -\frac{\mu^2}{(\partial \operatorname{Re}\epsilon_H/\partial\omega)_{\omega=\omega_H}(\partial \operatorname{Re}\epsilon_L/\partial\omega)_{\omega=\omega_L}} \tag{11}$$

is the dissipation free growth rate emerging from (2) by putting $\gamma_H \equiv \gamma_L = 0$. In (10) we considered the one-dimensional case where i denotes the relevant axis along which convection of modes takes place. For EBT experiments, because of relatively weak driver pump electric field available per section, the case of interest is the spatial growth rate less than the spatial damping rate of the low-frequency mode, Im k_H < Im $k_0 \ll$ Im k_L.

Finally, note that for the plasma modes and plasma parameters considered, the dispersion relation (1) represents a good approximation in the three frequency ranges studied here [for modification of (1) see, for example, Ref. (26)].

B. Some aspects of weak and strong parametric turbulence processes

Saturation of parametric instabilities in the weak turbulence theory approximation ($\gamma < \omega_L$, γ-parametric growth rate, and ω_L frequency of one of two parametrically excited modes with lower frequency) is fully described by the nonlinear wave kinetic equations[27,28]:

$$\hat{L}_H W_H(\mathbf{k},t) = 2\gamma(\mathbf{k})W_H(\mathbf{k},t) - 2\gamma_H^{\mathrm{NL}}(\mathbf{k})W_H(\mathbf{k},t), \tag{12}$$

$$\hat{L}_L W_L(\mathbf{k},t) = 2\gamma(\mathbf{k})W_L(\mathbf{k},t) - 2\gamma_L^{\mathrm{NL}}(\mathbf{k})W_L(\mathbf{k},t), \tag{13}$$

where the linear operator $\hat{L}_{H,L}$ is given by

$$\hat{L}_{H,L} \equiv \frac{\partial}{\partial t} + \mathbf{V}_{H,L}\frac{\partial}{\partial \mathbf{r}} + 2\gamma_{H,L}. \tag{14}$$

In (12) and (13) $W_{H,L}(\mathbf{k},t)$ are the spectral energy density of high- and low-frequency parametrically excited modes given by

$$W_{H,L}(\mathbf{k},t) = \frac{\partial}{\partial\omega}\left[\omega \operatorname{Re}\epsilon_{H,L}(\omega,\mathbf{k})\right]_{\omega=\omega_{H,L}(\mathbf{k})}\frac{E_{(H,L)0}^2}{16\pi}, \tag{15}$$

and the total energy density of the excited spectra by $W_{H,L} = \int d\mathbf{k}\, W_{H,L}(\mathbf{k})$. In (15), $E_{(H,L)0}$ is the electric field amplitude of the high- and low-frequency modes and $\omega_{H,L}(\mathbf{k})$ is the corresponding frequency spectrum. The source of parametric turbulence is described by the first term on the right-hand side of (12) and (13), where $\gamma(\mathbf{k})$ is the parametric growth rate describing primary decay of incoming radiation into two plasma modes.

Nonlinear dissipation of the excited H and L mode in (12) and (13) is modeled by $2\gamma_{H,L}^{\mathrm{NL}}(\mathbf{k})W_{H,L}(\mathbf{k})$, where $\gamma_{H,L}^{\mathrm{NL}}(\mathbf{k})$ represents the equivalent nonlinear damping rate. It describes the transfer of H (L) mode energy from the region of primary excitation $[\mathbf{k}d + \Delta\mathbf{k}, \omega(\mathbf{k}d) + \Delta\omega]$ into surrounding regions of $(\omega,\mathbf{k})$ space caused by the nonlinear interaction of waves. Here $\mathbf{k}d$ is the decay wave vector defined by $\omega_0(\mathbf{k}_0) = \omega_H(\mathbf{k}d) + \omega_L(\mathbf{k}d)$ and the quantities $\Delta\mathbf{k}, \Delta\omega$ depend on the primary parametric growth rate $\gamma(\mathbf{k}) \equiv \gamma_0(\mathbf{k})$. In our case of relatively weak driver pumps, the approximation of monochromatic primary parametric excitations, $|\Delta\mathbf{k}| \ll |\mathbf{k}d|$ and $\Delta\omega \ll \omega(\mathbf{k}d)$, is valid. Consequently, the total energy density of the excited spectrum is

$$\int_{\mathbf{k}d+\Delta\mathbf{k}} d\mathbf{k}\frac{\partial}{\partial\omega}\left[\omega_{H,L}(\mathbf{k})\operatorname{Re}\epsilon_{H,L}(\omega,\mathbf{k})\right]_{\omega=\omega_{H,L}(\mathbf{k})}$$

$$\times E_{(H,L)0}^2/16\pi \sim W_{H,L}(\mathbf{k}d). \tag{16}$$

In Sec. II B 1, it will be shown that because of the quasimonochromaticity of the primary parametric excitation, it is possible to model nonlinear wave interaction based on a power balance[29] treatment of (12) and (13).

The nonlinear terms in (12) have the explicit form (see, for example, Ref. 27)

$$
\begin{aligned}
&-2\gamma_H^{\mathrm{NL}}(\mathbf{k})W_H(\mathbf{k},t) \\
&\quad = -\frac{\omega_H(\mathbf{k})}{2\pi}\int d\mathbf{k}'\,d\mathbf{k}''\,Q_{HL}(\mathbf{k},\mathbf{k}',\mathbf{k}'')\delta(\mathbf{k}-\mathbf{k}'-\mathbf{k}'') \\
&\qquad \times[\omega_H(\mathbf{k})W_H(\mathbf{k}',t)W_L(\mathbf{k}'',t) \\
&\qquad -\omega_H(\mathbf{k}')W_H(\mathbf{k},t)W_L(\mathbf{k}'',t) \\
&\qquad -\omega_L(\mathbf{k}'')W_H(\mathbf{k},t)W_H(\mathbf{k}',t)]\,, \qquad (17)
\end{aligned}
$$

where $Q_{HL}(\mathbf{k},\mathbf{k}',\mathbf{k}'')$ is the kernel of nonlinear interaction of waves $\omega_H(\mathbf{k})$, $\omega_H(\mathbf{k}')$, and $\omega_L(\mathbf{k}-\mathbf{k}')$. The first term on the right-hand side of (17) describes the confluence interaction $\omega_H(\mathbf{k}')+\omega_L(\mathbf{k}'')\rightarrow\omega_H(\mathbf{k})$, and two others the decay interaction $\omega_H(\mathbf{k})\rightarrow\omega_H(\mathbf{k}')+\omega_L(\mathbf{k}'')$. A similar expression could be written for the low-frequency mode:

$$
\begin{aligned}
&-2\gamma_L^{\mathrm{NL}}(\mathbf{k}'')W_L(\mathbf{k}'',t) \\
&\quad = -\frac{\omega_L(\mathbf{k}'')}{2\pi}\int d\mathbf{k}'\,d\mathbf{k}''\,\delta(\mathbf{k}''+\mathbf{k}'-\mathbf{k})Q(\mathbf{k}',\mathbf{k},\mathbf{k}'') \\
&\qquad \times[\omega_L(\mathbf{k}'')W_H(\mathbf{k},t)W_H(\mathbf{k}',t) \\
&\qquad +\omega_H(\mathbf{k}')W_H(\mathbf{k},t)W_L(\mathbf{k}'',t) \\
&\qquad -\omega_H(\mathbf{k})W_L(\mathbf{k}',t)W_H(\mathbf{k}'',t)]. \qquad (18)
\end{aligned}
$$

Taking into account the Manley–Rowe relation $W_H/W_L \sim\gamma_L\omega_H/\gamma_H\omega_L$ (γ_L,γ_H damping rates of the low- and high-frequency mode) and because of the inequality $\gamma_L\gg\gamma_H$ valid in EBT plasmas, we can neglect W_L in (17), so that the dynamics of the high-frequency mode is not affected by the dynamics of the low-frequency mode. This, as will be shown in Sec. II B 1, enables us to treat the dynamics of the high-frequency mode [Eq. (12)] by a power balance equation.[24,25,29] A detailed treatment of (12) and (18) is given in Ref. 30 for the case of excitation of two Gould–Trivelpiece (G–T) modes or a G–T mode coupled to an ion-acoustic wave. According to Eq. (13), in the case of relatively weak driver pump (typical for EBT), we have $\gamma<\gamma_L(\mathbf{k})$, and consequently the dynamics of a low-frequency mode is completely described by linear theory, namely, it will dissipate linearly. The influence of low-frequency turbulence (or in other words ion nonlinearities) on the dynamics of parametrically excited high-frequency modes is beyond the scope of this paper. If $\gamma>\omega_L$ for the excited low-frequency mode, a description of saturation processes by (12) and (13) is not adequate. This is usually called strong turbulence regime[31] (see Sec. II B 2).

1. Stokes' line cascading and driver pump depletion

In the following, using as an example a LHW, we shall discuss weak and strong turbulence processes in a relatively weak driver pump electric field. In the regions where $\omega_0-\omega_{\mathrm{LH}}(r)\gg\omega_{\mathrm{IC}}$ (ω_{IC} is the frequency of an ion-cyclotron wave and ω_{LH} the frequency of a LHW) the dispersion of the LHW is strong (see Fig. 2) and, consequently, saturation of instabilities could be effectively governed by the secondary decays as a special case of weak turbulence processes.[27,28] The frequency spectrum of LHW has the form

$$
\omega_{\mathrm{LH}}=\omega_{\mathrm{LH}}^{*}(\mathbf{r})\left[1+\frac{1}{2}\left(\frac{k_z}{k}\right)^2\frac{m_i}{m_e}+\frac{3}{2}k^2\rho_e^2\frac{T_i}{T_e}\frac{\Omega_e\Omega_i}{\omega_{\mathrm{LH}}^2}\right], \qquad (19)
$$

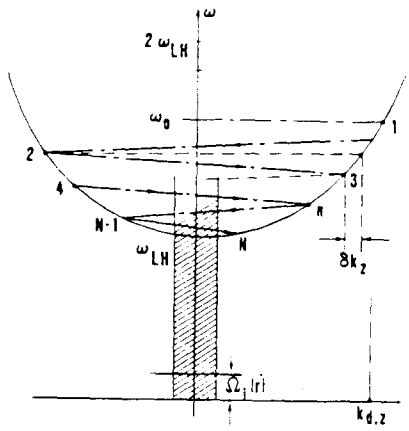

FIG. 2. Dispersion curve of cold lower-hybrid waves $\omega=\omega_{\mathrm{LH}}^{*}(r)\,[1+1/2(k_z/k)^2(m_i/m_e)]$. The numbers 1, 2, . . . ,n, . . . , $N-1$, N denote cascades, where N is the total number of cascades. The arrow shows the flow of energy of the driver pump into the condensated region (shaded area). Here $k_{d,z}$ is the decay wavenumber defining primary excitations given by (20).

and taking into account that $T_e\gtrsim 20\,T_i$ in EBT-S, we see that the third term in parentheses will not play any role in the cascading processes. This means that transfer of energy will go mainly through changes of k_z (see Fig. 2). In (19), $\omega_{\mathrm{LH}}^{*}=\omega_{pi}/(1+\omega_{pe}^2/\Omega_e^2)^{1/2}$, where ω_{pi} and ω_{pe} are the ion and electron plasma frequency, respectively. For the decay wavenumber we have

$$
\left(\frac{k_z}{k}\right)_d^2=\frac{2[\omega_0-\omega_{\mathrm{LH}}^{*}(r)]}{\omega_{\mathrm{LH}}^{*}(r)}\frac{m_e}{m_i}\,. \qquad (20)
$$

Expression (20) is evaluated under the assumption that $\omega_0-\omega_{\mathrm{LH}}^{*}(r)\gg\omega_{\mathrm{IC}}(r)$ (for EBT-S parameters $\omega_0-\omega_{\mathrm{LH(max)}}^{*}\lesssim 10\Omega_i$), which corresponds to the case of excitation of a well-defined ion-cyclotron wave. In the opposite case, $\omega_0-\omega_{\mathrm{LH}}^{*}(r)\ll\omega_{\mathrm{IC}}$, quasimodes[20] (especially if $T_e\sim T_i$) are excited. They have, however, in principle, higher thresholds and are not of interest for weak driver pumps (see Ref. 20). We note that once excited their growth rates could be larger than the growth rates of well-defined modes.

Primary excited lower-hybrid waves decay further into other LHW coupled to ion-cyclotron waves, etc. It is to be noted that cascade saturation mechanisms always take place in regions whose location with respect to the resonance surface is given by $\Delta=\omega_0-\omega_{\mathrm{LH}}(r)\gg\omega_{\mathrm{IC}}$, as mentioned earlier. Such a frequency mismatch gives a primary excited mode with strong dispersion and, accordingly, its energy is dissipated effectively through cascade energy transfer into the regions of lower $|\mathbf{k}|$ (see Fig. 2). The frequency spectrum of cascades is given by

$$
\omega_{\mathrm{LH}}^{(n)}(k_{z,\mathrm{LH}}^{(n)})=\omega_0-\sum_{m=1}^{n}\omega_{\mathrm{IC}}^{(m)}(k_{z,\mathrm{IC}}^{(m)}), \qquad (21)
$$

$$
k_{z,\mathrm{LH}}^{(n)}=(-1)^{n-1}[k_{z,d}-(n-1)\delta k_{z,\mathrm{LH}}]. \qquad (22)
$$

Here n denotes the cascade number and $\omega_{\mathrm{IC}}^{(m)}$ is the frequency of the ion-cyclotron wave in the mth cascade. The wavenumber spacing between cascades, δk_z, is given by (Fig. 2)

$$
\frac{\delta k_{z,\mathrm{LH}}}{k_d^2}\sim\frac{2\omega_{\mathrm{IC}}(2k_{z,d})}{2\omega_{\mathrm{LH}}k_{z,d}}\frac{m_e}{m_i}\,. \qquad (23)
$$

The total number of cascades is found to be

$$N = \min\left\{\frac{\gamma}{\gamma_{LH}}, \frac{\omega_0 - \omega_{LH}(r)}{\Omega_i(r)}\right\}. \tag{24}$$

Here $\Omega_i(r)$ is the local ion-cyclotron frequency. The first term in the bracket in (24) is the known result of power balance theory (see Ref. 10) and the second one is specific for LHFR. If $\gamma \gtrsim \gamma_{LH}$ (the case of relatively strong driver pumps), then the maximum number of cascades is $N \lesssim \omega_{LH}(r)/\Omega_i(r)$ [$\omega_0 \lesssim 2\omega^*_{LH}(r)$; in the opposite case parametric processes are ineffective].[20,30]

Taking into account (21) and (22), we can transform Eq. 12) to describe the k-space-time evolution of the nth cascade. In doing this, we have to make the following substitution: $\hat{L}\, W_{LH} \equiv \hat{L}\, W^{(n)}_{LH}$; $2\gamma(\mathbf{k}) W_{LH}(\mathbf{k}) \equiv 2\gamma^{n-1}(\mathbf{k}^{(n-1)})\, W^{(n)}_{LH}(\mathbf{k})$ and $2\gamma_{NL}(\mathbf{k}) W_{LH}(\mathbf{k}) \equiv \gamma^{(n)}(\mathbf{k}^{(n)}) W^{(n+1)}_{LH}(\mathbf{k}^{(n+1)})$. As a consequence, we obtain a system of power balance equations in the form

$$\begin{aligned}
&\frac{\partial W_1}{\partial t} = 2\gamma_0 W_1 - 2\gamma_{LH} W_1 - 2\gamma_1 W_2,\\
&\frac{\partial W_2}{\partial t} = 2\gamma_1 W_2 - 2\gamma_{LH} W_2 - 2\gamma_2 W_3,\\
&\quad\cdots\\
&\frac{\partial W_N}{\partial t} = 2\gamma_{N-1} W_{N,THR} - 2\gamma_{LH} W_{N,THR}\,.
\end{aligned} \tag{25}$$

A description of weak turbulence processes by system (25) is valid only in the case where the k-space width of a cascade is small compared to k spacing between cascades. In other words, the growth rate has to be small, $\gamma < \gamma_{IC}$ (γ_{IC} linear damping rate of the ion-cyclotron wave), which is satisfied for EBT's relatively weak electric fields. As a consequence, a line-like turbulence spectrum is to be expected in these experiments. A detailed treatment of system (25) is given in Ref. 10. The last equation in (25) is written under the assumption that the deposited driver pump energy goes completely into weak turbulence. However, if the total number of cascades is large enough, a significant amount of power will be transferred to a strong turbulence region (condensate region) which now plays the role of a second channel for power deposition (see Sec. II B 2).

As seen from (25), in a quasistationary state ($\partial/\partial t \sim 0$), the saturation of each cascade will be governed by the convective term $\mathbf{V}_H(\partial/\partial \mathbf{r}) W_{LH}$ and by the nonlinear term $2\gamma_{NL} W_H$. The influence of the convective term on the cascading saturation mechanism is strong if $V_H/L_N \gtrsim \gamma_{NL}$ (L_N is the local plasma inhomogeneity scale length in the relevant direction). The influence of convection of waves on saturation is treated in Ref. 10, where expressions for absorbed energy and absorption rates were obtained. If $V_H/L_N \gg \gamma_{NL}$, then saturation of parametrically excited waves is completely governed by convection. This occurs in the case of extremely weak driver pumps and high group velocity of excited waves. The amplitude of the convecting wave is finally saturated by depletion of the driver.[32]

Let us now consider the nth cascade in (25). In the stationary state we have

$$\gamma_{n-1} W_n = \gamma_{LH} W_H - \gamma_n W_{n+1}. \tag{26}$$

Taking into account the dependence of γ_n on W_n [see Eqs. (2), (3), and (8)] from (26), we obtain the simple differential equation

$$-\frac{dW_n}{dn} = \frac{\gamma_H}{\gamma_0}\frac{A_0}{A_n} W_0. \tag{27}$$

Equation (27) is obtained under the assumption of parametric excitation of a low-frequency quasimode when $\gamma_H < \gamma_0 < \gamma_L$ is satisfied (γ_0 is the primary growth rate). In (27) we have also utilized the fact that, in the weak driver pump approximation, parametric growth rates can be expressed in terms of the wave energy density in the form $\gamma_0 = A_0 W_0$ and $\gamma_n = A_n W_n$ [see Eq. (2)]. Here γ_n is the growth rate of the nth cascade, and W_0 and W_n are the energy densities of a driver pump and the nth cascade given by (resonant case)[18]

$$W_{0,n} = \left(\omega \frac{\partial\, \mathrm{Re}\, \epsilon_H}{\partial \omega}\right)_{\omega=\omega_H} \frac{E^2_{0,n}}{16\pi}. \tag{28}$$

In the case of excitation of well-defined low-frequency modes ($\gamma_L \ll \omega_L$, $\gamma_0 > \gamma_L$) by relatively weak driver pumps, the dynamics of high-frequency cascades is described by

$$-\frac{d}{dn}(W_n)^{1/2} = \frac{\gamma_H}{\gamma_0}\frac{B_0}{B_n}(W_0)^{1/2}. \tag{29}$$

Here we have utilized the relations $\gamma_0 = B_0(W_0)^{1/2}$ and $\gamma_n = B_n(W_n)^{1/2}$. Integration of (28) and (29) gives the turbulence spectrum in the forms

$$\begin{aligned}
&W_n = \frac{\gamma_H}{\gamma_0}\frac{A_0}{A_n} W_0(N-n) + W_{0,THR},\\
&n = 1,2,\ldots,N, \quad \gamma_H < \gamma < \gamma_L,
\end{aligned} \tag{30}$$

$$\begin{aligned}
&W_n = \left(\frac{\gamma_H}{\gamma_0}\right)^2 \left(\frac{B_0}{B_n}\right)^2 W_0(N-n)^2,\\
&n = 1,2,\ldots,N, \quad \gamma > \gamma_H, \gamma_L\,.
\end{aligned} \tag{31}$$

As seen from (30) and (31), the turbulence spectra are discrete (line-like), which is a consequence of the assumption that γ_0, $\gamma_n \ll \omega_L$ (weak parametric turbulence approximation). If γ_0, $\gamma_n \lesssim \omega_L$, a strong interaction between cascades takes place and the description of cascade dynamics by (27) and (29) is no longer valid. In (30) and (31), N is the total number of cascades that can be easily found from the equation (this is equivalent to demanding that the intensity of the last, nth, cascade be equal to the threshold value)

$$\gamma_0 W_1 = \sum_{n=1}^{N} \gamma_H W_n\,, \tag{32}$$

to be

$$N \sim 2(\gamma_0/\gamma_H)(A_N/A_1), \quad \gamma_H < \gamma < \gamma_L\,, \tag{33}$$

$$N \sim 3(\gamma_0/\gamma_H)(B_N/B_1)^2, \quad \gamma > \gamma_H, \gamma_L\,. \tag{34}$$

It is to be noted that results (33) and (34) are not general and, as seen from (24), they are modified in the lower-hybrid frequency range. The parametric turbulence level is defined by $W_{TURB}/n_e T_e$, where

$$W_{TURB} = 2\sum_{n=1}^{N} W_n, \tag{35}$$

and n_e, T_e are the electron density and electron temperature in energy units, respectively. The factor of 2 in the expression for W_{TURB} comes as a consequence of the simultaneous excitation of two high-frequency waves with inverse wave vectors. A simple algebraic calculation leads to the final forms

$$W_{\mathrm{TURB}} \sim 4\left(\frac{A_0}{A_1}\frac{A_N}{A_1}\frac{\gamma_0}{\gamma_H} W_0 + \frac{\gamma_0}{\gamma_H}\frac{A_N}{A_1} W_{0,\mathrm{THR}}\right),$$
$$\gamma_H < \gamma < \gamma_L, \tag{36}$$

$$W_{\mathrm{TURB}} \sim 18\left(\frac{B_0}{B_1}\right)^2\left(\frac{B_N}{B_1}\right)^4\frac{\gamma_0}{\gamma_H} W_0,$$
$$W_{0,\mathrm{THR}} \ll W_{\mathrm{TURB}}, \quad \gamma > \gamma_H, \gamma_L. \tag{37}$$

Taking into account that $W_{0,\mathrm{THR}}/W_0 = \gamma_H/\gamma_0$ if $\gamma_H < \gamma_0 < \gamma_L$ [see Eq. (2)], the turbulence energy density can be expressed in a convenient form in terms of the threshold energy density:

$$W_{\mathrm{TURB}} \sim 4\frac{\mu_L^4}{\gamma_L^2\gamma_H^2}\left(\frac{\partial \operatorname{Re}\epsilon_H}{\partial\omega}\right)^{-2}_{\substack{\omega=\omega_H\\ \mathbf{k}=\mathbf{k}_H}}\left(\frac{\partial \operatorname{Re}\epsilon_L}{\partial\omega}\right)^{-2}_{\substack{\omega=\omega_L\\ \mathbf{k}=\mathbf{k}_L}}$$
$$\times\left(\frac{A_0}{A_1}\right)\left(\frac{A_N}{A_1}\right) W_{0,\mathrm{THR}}, \quad \gamma_H < \gamma_0 < \gamma_L. \tag{38}$$

If the low-frequency mode is weakly damped ($\gamma_0 > \gamma_L$), we have from (2),

$$W_{0,\mathrm{THR}}/W_0 = \gamma_L\gamma_H/\gamma_0^2. \tag{39}$$

Repeating the above procedure for the turbulence energy density, we obtain

$$W_{\mathrm{TURB}} \sim 18\frac{\mu_L^3}{\gamma_H^2\gamma_L}\left(\frac{\partial \operatorname{Re}\epsilon_H}{\partial\omega}\right)^{-3/2}_{\substack{\omega=\omega_H\\ \mathbf{k}=\mathbf{k}_H}}\left(\frac{\partial \operatorname{Re}\epsilon_L}{\partial\omega}\right)^{-3/2}_{\substack{\omega=\omega_L\\ \mathbf{k}=\mathbf{k}_L}}$$
$$\times\left(\frac{B_0}{B_1}\right)^2\left(\frac{B_N}{B_1}\right)^4 W_{0,\mathrm{THR}}, \quad \gamma_0 \gg \gamma_H, \gamma_L. \tag{40}$$

The importance of secondary decays is determined by the ratios (A_0/A_1) and (B_0/B_1). If primary and secondary decays are not of the same nature, then $A_1 > A_0$ and $B_1 > B_0$, which can significantly reduce turbulence levels (38) and (40). In the opposite case, $B_0 \lesssim B_1$ and $A_0 \lesssim A_1$.

The case of excitation of two high-frequency modes could be treated based on (40). Now, the right-hand side of (37) is to be multiplied by 2 to include the existence of two high-frequency modes. Further, the substitutions $\mu_L \to \mu_H$, $\epsilon_L \to \epsilon_H$, and $\gamma_L \to \gamma_H$ are to be made. Accordingly,

$$W_{\mathrm{TURB}} \sim 36\frac{\mu_H^3}{\gamma_H^3}\left(\frac{\partial \operatorname{Re}\epsilon_H}{\partial\omega}\right)^{-3}_{\substack{\omega=\omega_H\\ \mathbf{k}=\mathbf{k}_H}}\left(\frac{B_0}{B_1}\right)^2\left(\frac{B_N}{B_1}\right)^4 W_{0,\mathrm{THR}}. \tag{41}$$

It will be shown in Sec. II B 3 that the expressions (38), (40), and (41) play crucial roles in the calculation of nonlinearly absorbed energy.

Writing (12) for the pump in the stationary state we have

$$V_0\frac{\partial}{\partial \mathbf{r}} W_0 = -2\gamma_0 W_1 = -2\gamma_H W_{\mathrm{TURB}}^{\mathrm{conv}},$$
$$W_{\mathrm{TURB}}^{\mathrm{conv}} = 2\sum_{n=1}^{N} W_n^{\mathrm{conv}}, \tag{42}$$

and for the first cascade in the case of convective instability [compare to (26)]

$$\operatorname{Im} k_0 V_{\mathrm{LH}} W_1 = 2\operatorname{Im} k_{\mathrm{LH}} V_{\mathrm{LH}} W_1 - 2\operatorname{Im} k_1 V_{\mathrm{LH}} W_2, \tag{43}$$

where the subscript 0 denotes the pump, $\operatorname{Im} k_1$ is the imaginary part of the wavenumber in the first cascade, and $\operatorname{Im} k_{\mathrm{LH}}$ is the spatial damping rate of LHW. If secondary and primary decays are of the same nature, then in (43), $W_1 \sim W_2$ and W_1 can be found from $\operatorname{Im} k_0 \sim 2\operatorname{Im} k_1$. Then combining (42) and (43), we can define the driver pump depletion length L at which all power is absorbed by the plasma:

$$V_{0i} W_0(0) = -2\int_0^L \operatorname{Im} k_{\mathrm{LH}} V_{\mathrm{LH}} W_{\mathrm{TURB}}^{\mathrm{conv}}\, di, \tag{44}$$

where i denotes the direction of convection. In the first approximation, from (44) we have

$$L^{\mathrm{conv}} = \frac{V_{0,i}}{2\operatorname{Im} k_{\mathrm{LH}} V_{\mathrm{LH}}}\frac{W_0(0)}{W_{\mathrm{TURB}}^{\mathrm{conv}}(0)}, \tag{45}$$

where 0 denotes the reference surface. Equation (45) could be written in a somewhat different form:

$$L^{\mathrm{conv}} = \frac{V_{0,i}}{2\operatorname{Im} k_0 V_{\mathrm{LH}}}\frac{W_0(0)}{W_1^{\mathrm{conv}}(0)}. \tag{46}$$

The term $W_{\mathrm{TURB}}^{\mathrm{conv}}$ is derived in Ref. 10 for the case of well-defined modes and quasimodes.

2. Lower-hybrid wave condensate

From Fig. 2 it can be seen that through cascading processes a significant amount of energy (if $\gamma \gg \gamma_{\mathrm{LH}}$) could be deposited in the condensate region, $k_z \sim 0$ and, consequently, $V_{\mathrm{LH}} \sim 0$. In this region (shaded area in Fig. 2), secondary decays are not possible because of the impossibility of satisfying selection rules. Accordingly, all energy of LHW with wave vectors perpendicular to $\mathbf{B}_0$, $k_z \to 0$, will be stored in the form of LHW condensate where strong turbulence[31] saturation mechanisms take place.

A condensate region can be described by power balance equations:

$$\frac{\partial}{\partial t} W_{\mathrm{cond}} = P^{\mathrm{ST}} - 2\gamma_{\mathrm{LH}}^{\mathrm{coll}} W_{\mathrm{cond}} - 2\gamma_{\mathrm{mod}} W_{\mathrm{cond}} - 2\gamma^{\mathrm{WW}} W_{\mathrm{cond}}, \tag{47}$$

$$\frac{\partial}{\partial t} W_{\mathrm{SH}} = 2\gamma_{\mathrm{mod}} W_{\mathrm{SH}} - 2\gamma_{\mathrm{LH}}^{\mathrm{noncoll}} W_{\mathrm{SH}}. \tag{48}$$

Here W_{cond} is the energy density in the condensate region and W_{SH} is the energy density in the short-wavelength regions as a consequence of nonlinear evolution of modulation instabilities.[31] This leads to the transfer of energy from long-wavelength regions into short-wavelength regions ($k_z \gg k_{0z}$). Here γ_{mod} and γ^{WW} are the growth rates of modulation instability[31] and of decay of LHW into whistler waves coupled to some low-frequency mode,[33] and P^{ST} denotes the power density transferred from the weak turbulence region into the condensate region (see Fig. 2). It is evident that if $P^{\mathrm{WT}} \sim 0$, the condensate of LHW will not be formed. However, if $\gamma/\gamma_{\mathrm{LH}} > [\omega_0 - \omega_{\mathrm{LH}}(r)]/\Omega_i(r)$, then part of the energy from

the weak turbulence region will be transferred to the strong turbulence region (condensate). In high-temperature plasma, $\gamma_{\rm coll}^{\rm LH} \sim 0$, the energy in the condensate region will be transferred into the short-wavelength region, if $\gamma_{\rm mod} \gg \gamma^{\rm WW}$, leading to the appearance of suprathermal electrons.[34] In the opposite case, $\gamma^{\rm WW} \gg \gamma_{\rm mod}$, energy will be irradiated through whistlers. To determine what channel will be preferential in the condensate region requires separate consideration and is not in the scope of this paper.

Power balance gives $P_0 = P^{\rm WT} + P^{\rm ST}$, where P_0 is the power of the driver pump, $P^{\rm WT}$ the power of the weak turbulence region, and $P^{\rm ST}$ the power transferred from the weak turbulence region into the strong turbulence region (Fig. 2). Consequently, $P_0 = P^{\rm WT}(1+\alpha)$, where $\alpha \equiv 0$ if $\gamma_0/\gamma_{\rm LH} < [\omega_0 - \omega_{\rm LH}(r)]/\Omega_i(r)$ and $\alpha = P^{\rm ST}/P^{\rm WT}$ if $\gamma_0/\gamma_{\rm LH} > [\omega_0 - \omega_{\rm LH}(r)]/\Omega_i(r)$. Here we have assumed that total external power flows through primary and secondary decays in the weak turbulence domain ($k_d \gg k_0$). Using (24), (47), and (48) in stationary phase we have

$$\alpha \equiv \frac{P^{\rm ST}}{P^{\rm WT}} = \frac{\gamma^{\rm WW}}{\gamma_{\rm LH}(k \sim k_d)} \left(\frac{\gamma_0}{\gamma_{\rm LH}} \frac{\Omega_i}{\omega_0 - \omega_{\rm LH}(r)} - 1 \right). \quad (49)$$

This expression gives the ratio of power deposition in strong and weak turbulence regions under the assumption that the main saturation process in the condensate region is the decay LHW$\rightarrow$WW + L [in (47) $\gamma_{\rm coll}^{\rm LH} \sim 0$, $\gamma_{\rm mod} \sim 0$], where L denotes some low-frequency mode. If, however, modulation instability evolves in the condensate region ($\gamma_{\rm mod} \gg \gamma^{\rm WW}$), then in (49) $\gamma^{\rm WW}$ is to be replaced by $\gamma_{\rm mod}$. In the EBT-S environment, as seen from (49), the transfer of energy from a weak turbulence domain into a strong turbulence domain takes place if $\gamma_0/\gamma_{\rm LH} > 20$, which is easily satisfied for collisionally damped, primary excited ($k_d < k_{\rm coll}$) LHW or for relatively stronger driver pumps.

3. Anomalous absorption

A quantitative description of the nonlinear dissipation of the electric field energy of a driver pump is based on the anomalous absorption frequency (ν_a) and the anomalous absorption length (L_a). The anomalous absorption frequency is used as a local absorption characteristic through the expression $\nu_a (E_0^2/8\pi)$, representing the nonlinearly dissipated external energy per unit time and volume. The anomalous absorption length represents the length over which the total external energy is nonlinearly absorbed: $L_a = c/\nu_a$ in ECFR [see (45)]. It is obvious that $\nu_a W_0 = 2\gamma_0 W_1$. The energy content in the first cascade (W_1) could be found, neglecting linear dissipation, from the equation

$$\gamma_0(W_0) W_1 = \gamma_1(W_1) W_2. \quad (50)$$

In the first approximation, $W_1 \sim W_2$, which gives $W_1 = f(W_0)$. If primary and secondary decays are of the same nature, then $W_1 \sim W_0$. Finally, for the nonlinear absorbed power density we obtain

$$Q = 2\gamma_1(W_1) f(W_0). \quad (51)$$

From (51) a crucial role of secondary decay is evident. If primary and secondary decays are of the same nature, a known result[35,36] $Q = 2\gamma_0 (E_0^2/8\pi)$, could be obtained from (51). Another way of defining the absorbed power density is by means of the turbulence energy density in the form

$$Q = 2\gamma_H W_{\rm TURB}. \quad (52)$$

From (38), (40), (41), and (52), it is evident that the effectiveness of the cascade saturation mechanism strongly depends on linear dissipation of the high-frequency mode. This mechanism is definitely most effective in the case of extremely small linear damping rates of excited high-frequency waves [see (40) and (41)]. This is true, for example, in fusion plasmas for predominant collisional dissipation of excited waves with decay wave vectors $\mathbf{k}_d$ satisfying $|\mathbf{k}_d| \ll k_{\rm coll}$, where the collisional wavenumber $k_{\rm coll}$ is obtained by equating collisional and noncollisional dissipation. For excitations in which excited waves have significant Landau or cyclotron damping, the effectiveness of the saturation mechanism remains if the driver pump electric field is correspondingly increased.

It is easy to show that the dynamics of high-frequency cascades in the case of convective instability are described by (27) and (29) if the formal substitution $\gamma_0 \rightarrow {\rm Im}\, k_0 V_H$ is made [see (43)].

In the case of excitation of the well-defined low-frequency mode ($\gamma_L \ll \omega_L$, $\gamma_0 > \gamma_L$) as convective instability for the absorbed power density $Q^{\rm conv} = 2\,{\rm Im}\, k_0 V_H W^{\rm conv}$, we have

$$Q^{\rm conv} = 18 \frac{\mu_L^4}{\gamma_L^2 \gamma_H} \left(\frac{\partial\, {\rm Re}\, \epsilon_H}{\partial \omega} \right)_{\omega=\omega_H}^{-2} \left(\frac{\partial\, {\rm Re}\, \epsilon_L}{\partial \omega} \right)_{\omega=\omega_L}^{-2} \times \left(\frac{B_0}{B_1} \right)^2 \left(\frac{B_N}{B_1} \right)^4 W_{0,\rm THR}, \quad \gamma_0 > \gamma_H, \gamma_L. \quad (53)$$

Here we took into account that

$${\rm Im}\, k_0 = \gamma_{d0}^2/(V_H V_L\, {\rm Im}\, k_L), \quad (54)$$

where ${\rm Im}\, k_L = \gamma_L/V_L$. It is to be noted that (53) is valid for electric field intensities satisfying $\gamma^2 \gg \gamma_H \cdot \gamma_L$ and $\gamma \ll \gamma_L \times (V_H/V_L)^{1/2}$. Comparison of (53) with $Q^{\rm ABS} = \gamma_H W_{\rm TURB}^{\rm ABS}$ [see (40)] shows that nonlinearly absorbed energy in the case of convective instabilities is (γ_0/γ_L) times larger than in the case of the absolute instability if the saturation mechanism is cascading.

If heavy damped modes ($\gamma_L \lesssim \omega_L$, $\gamma_0 < \gamma_L$) are excited,

$${\rm Im}\, k_0 = \gamma_0/V_H, \quad (55)$$

and, consequently,

$$Q^{\rm conv} = 4 \frac{\mu_L^4}{\gamma_L^2 \gamma_H} \left(\frac{\partial\, {\rm Re}\, \epsilon_H}{\partial \omega} \right)_{\omega=\omega_H}^{-2} \left(\frac{\partial\, {\rm Re}\, \epsilon_L}{\partial \omega} \right)_{\omega=\omega_L}^{-2} \times \left(\frac{A_0}{A_1} \right) \left(\frac{A_N}{A_1} \right) W_{0,\rm THR}, \quad \gamma_H < \gamma_0 < \gamma_L. \quad (56)$$

Additional restriction for the validity of (56) is the inequality $\gamma_0 < \gamma_L (V_H/V_L)$. Comparison of (56) with $Q^{\rm ABS} = \gamma_H W_{\rm TURB}^{\rm ABS}$ [see (38)] shows that in the case of the heavily damped mode, the nonlinearly absorbed energy is the same for convective and absolute instabilities. Note that although in the inhomogeneous plasma excitation of quasimodes always appears to be convective, it is not true when inhomoge-

neity of the pump and plasma are simultaneously taken into account.[23] In this case, the formal substitution $\gamma_0 \rightarrow \mathrm{Im}\, k_0 V_H$ becomes an identity [see (55)] and all results for the case of absolute instabilities could be directly applied for the convective instabilities.

For the case of excitation of two high-frequency modes we have

$$Q^{\mathrm{conv}} = 36 \frac{\mu_H^4}{\gamma_H^3} \left(\frac{\partial\, \mathrm{Re}\, \epsilon_H}{\partial \omega} \right)^{-4}_{\omega=\omega_H} \left(\frac{B_0}{B_1} \right)^2 \left(\frac{B_N}{B_1} \right)^4 W_{0,\mathrm{THR}} . \tag{57}$$

It is evident that (57) could be obtained from (53), multiplying by two and substituting $\mu_L \rightarrow \mu_H$, $\epsilon_L \rightarrow \epsilon_H$, $\gamma_L \rightarrow \gamma_H$, and $V_L \rightarrow V_H$.

III. ELECTRON-CYCLOTRON HARMONIC RESONANCES

In the standard theory of linear resonance heating in EBT, the second electron-cyclotron harmonic resonance layer is located in the low-field side and the principal harmonic layer in the high-field side, respectively, as shown in Fig. 1. Being launched from the low-field side (radial launching), the X or O mode first reaches the second electron-cyclotron harmonic layer (ring heating zone) where it is partly absorbed. In this layer, as will be shown later, excitation of two electron-cyclotron or two upper-hybrid waves is possible, as well as excitation of a second harmonic EC wave coupled to low-frequency modes. Having passed through the second electron-cyclotron harmonic (SECH) layer on the outer side of EBT, the driver pump then reaches the SECH layer on the inner side of EBT where, again, it is partly absorbed. As seen from Fig. 3 for EBT-S parameters, the right-hand cutoff surface is absent between two SECH layers. The remaining EM radiation is reflected from the inner wall of EBT in the form of the X and O mode and approaches the principal harmonic layer (core plasma heating zone). In this layer, excitation of a principal harmonic electron-cyclotron wave coupled to low-frequency modes is possible by the O-mode component. In recent literature, absorption processes in EBT are treated as linear in both ring and core heating zones. However, as will be shown for both ring and core heating zones, parametric processes can take place under certain conditions. Accordingly, in both wave propagation and absorption calculations, nonlinear processes must be taken into account in explaining experimental results.[12,13]

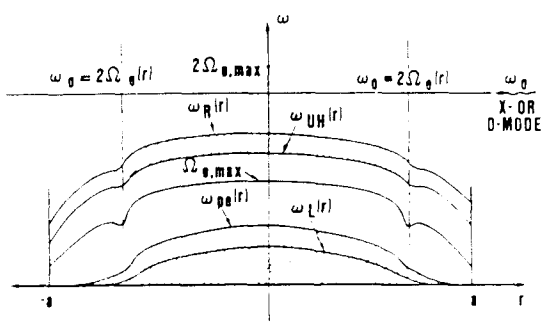

FIG. 3. Radial launching of X and O mode (r is the midplane radius). Right-hand and left-hand cutoff frequencies of X mode are denoted by ω_R and ω_L and are given by $\omega_{R,L} = \pm \Omega_e/2 + (\Omega_e^2/4 + \omega_{pe}^2)^{1/2}$. The cutoff frequency for the O mode is $\omega \equiv \omega_{pe}$. The figure is constructed for EBT-S with $\Omega_e \sim 1.5\omega_{pe}$. Shaded areas denote cutoff regions.

We shall study the excitation of plasma modes with frequencies near the local electron-cyclotron harmonic frequency. Let us first consider simultaneous excitation of two electron-cyclotron harmonic waves (electron Bernstein modes) with frequency spectrum given by Eq. (A4) and corresponding dielectric permittivity by (A3). The geometry of the interaction is defined by the wave vector of the low-frequency mode $\mathbf{k} = \{0, k_y, k_z\}$ ($k_z/k_y \ll 1$, nearly perpendicular propagation), driver pump electric field $\mathbf{E}_0 = \{0, E_{0y}, 0\}$ (in vacuum for X mode), magnetic field vector $\mathbf{B}_0 = \{0,0,B_0\}$, and the driver pump wave vector $k_0 = \{k_{0x}, 0, k_{0z}\}$ (in vacuum for nearly perpendicular incidence $k_{0z}/k_{0x} \ll 1$). Based on known formalism[16] for the coupling coefficient, we obtain

$$\mu_{H,1}^2 = \frac{e^2 E_{0y}^2 k_y^2}{m_e^2 [\phi(S)]^2} \left[1 + \left(\frac{\Omega_e}{\omega_0} \right)^2 \left(\frac{k_{0x}}{k_y} \right)^2 \right] \times \frac{(2k_z k_{0z} - k_{0x}^2 - k_{0z}^2)^2}{(k_y^2 + k_z^2)[k_{0x}^2 + k_y^2 + (k_z - k_{0z})^2]} . \tag{58}$$

In (58) the function $\phi(S)$ is given by (A8). It is evident from (58) that the crucial role in this kind of parametric excitation is played by the finite wavelength of the driver pump.[8,16,37] In the case of simultaneous excitation of lth and mth harmonic electron Bernstein modes (EBM) for the parametric growth rate we have [$\omega_0 = (l+m)\Omega_e = S\Omega_e$]

$$(\gamma + \gamma_{\mathrm{EB}}^{(l)})(\gamma + \gamma_{\mathrm{EB}}^{(m)}) = \mu_H^2 \frac{lm\Omega_e^2}{\omega_{pe}^4} k^4 \rho_e^4 \times \left(\sum_{l=-\infty}^{+\infty} \sum_{m=-\infty}^{+\infty} \frac{(lm)^2 A_l(k_\perp^2 \rho_e^2) A_m(k_\perp^2 \rho_e^2)}{(\omega^{(l)} - l\Omega_e)^2 (\omega^{(m)} - m\Omega_e)^2} \right)^{-1} . \tag{59}$$

In (59), $\gamma_{\mathrm{EB}}^{(l,m)}$ is the linear damping rate of EBM, which in the case of perpendicular propagation [$k_z/k \ll (m_e/m_i)^{1/2}$] is given by (A7). Here ρ_e is the electron Larmor radius and $A_n(x) = I_n(x)e^{-x}$, where I_n is the modified Bessel function of the first kind of order n. In (59) $\omega^{(l,m)}$ is given by (A4).

In the EBT environment, expression (59) could be directly applicable if $l = m = 1$, which corresponds to excitation of two principal harmonic EBM in the second electron-cyclotron harmonic resonance layer (see Fig. 1). Accordingly, from (59) we obtain

$$(\gamma + \gamma_{\mathrm{EB}}^{(1)})^2 = \mu_{H,1}^2 \frac{k^4 r_{De}^4 \Omega_e^2 A_1^2(k_\perp^2 \rho_e^2)}{[1 + k^2 r_{De}^2 - A_0(k_\perp^2 \rho_e^2)]^4} , \tag{60}$$

with

$$\mu_{H,1}^2 = \frac{E_{0y}^2}{36\pi n_e T_e} \left(\frac{\omega_{pe}}{\Omega_e} \right)^4 \left[1 + \left(\frac{\Omega_e}{\omega_0} \right)^2 \left(\frac{k_{0x}}{k_y} \right)^2 \right] (k_y r_{De})^2 \times \frac{(2k_{0z}k_z - k_{0x}^2 - k_{0z}^2)^2}{[k_{0x}^2 + k_y^2 + (k_z - k_{0z})^2](k_y^2 + k_z^2)} . \tag{61}$$

For the corresponding electric field threshold value, we have

$$\frac{E_{0y}^{T}}{(4\pi n_e T_e)^{1/2}} = \frac{3[1+k^2 r_{De}^2 - A_0(k_\perp^2 \rho_e^2)]^2}{A_1(k_\perp^2 \rho_e^2)} \times\left(\frac{\Omega_e}{\omega_{pe}}\right)^2\left[1+\left(\frac{k_y}{k_{0x}}\right)^2\right]^{1/2} \times(k_{0x} r_{De})^{-1}(k r_{De})^{-2}\left[1+\left(\frac{\Omega_e}{\omega_0}\right)^2 \times\left(\frac{k_{0x}}{k_y}\right)^2\right]^{-1/2}\frac{V_{EB}^{(1)}}{L_y \Omega_e}. \quad (62)$$

Here we have assumed, for the sake of simplicity, perpendicular incidence ($k_{0z}=0$) and strictly perpendicular propagation of the EBM. In (60) and (62) $\gamma_{EB}^{(1)}$ is the linear damping rate of the principal harmonic electron Bernstein mode, given by ($l=1$):

$$\gamma_{EB}^{(l)} = -\frac{\operatorname{Im}\epsilon_{EB}}{(\partial \operatorname{Re}\epsilon_{EB}/\partial\omega)_{\omega=l\Omega_e}}, \quad (63)$$

(for ϵ_{EB}, see the Appendix) which, in the case of nearly perpendicular propagation [$k_z/k \ll (m_e/m_i)^{1/2}$], includes only collisions [see (A7)]. If $k_z/k > (m_e/m_i)^{1/2}$, noncollisional damping of EBM is to be taken into account, which can enhance the dissipative threshold several times. The expression (62) gives the threshold caused by the plasma inhomogeneity along the y axis, with L_y given by

$$L_y = \left(\frac{2\pi}{(\partial \Delta k_y/\partial y)}\right)^{1/2}, \quad (64)$$

where Δk_y is the mismatching quantity equal to $|\Delta\mathbf{k}(y)| = |\mathbf{k}_0(y) - \mathbf{k}_{EB}^{(1)}(y) - \mathbf{k}_{EB}^{(2)}(y)|$. Here $\mathbf{V}_{EB}$ is the group velocity of the EBM, which is given by

$$\mathbf{V}_{EB}^{(l)} = l|\Omega_e|\frac{\partial}{\partial \mathbf{k}}\left(\frac{A_l(k_\perp^2\rho_e^2)}{1+k^2 r_{De}^2 - A_0(k_\perp^2\rho_e^2)}\right). \quad (65)$$

In (62) we shall assume $k\rho_e \sim k_y\rho_e \sim 0.1$, which for ORNL gyrotrons ($f_0 = 10.6$; 28 GHz, $k_0 \sim 3.3$–$5.6\ \mathrm{cm}^{-1}$) gives $k_y \geqslant 10\ \mathrm{cm}^{-1}$ ($\rho_e \lesssim 10^{-2}$ cm) and $k_y > k_{0x}$. Accordingly, we have

$$\frac{E_{0y}^{T}}{(4\pi n_e T_e)^{1/2}} = 6\left(\frac{\Omega_e}{\omega_{pe}}\right)^4 \frac{k_y}{k_{0x}^2 r_{De}} \frac{V_{EB}^{(1)}}{L_y \Omega_e}, \quad k_y^2\rho_e^2 \ll 1. \quad (66)$$

For typical parameters of EBT-S ($\Omega_e/\omega_{pe} \sim 1.58$, $\rho_e/L_y \sim \rho_e/10\lambda_0 \gtrsim 10^{-4}$, $k_y r_{De} \sim 0.2$), from (66) we have $E_{0y}^{T} \gtrsim 350$ V/cm for $V_{EB}^{(1)} \sim 10^{-1} V_{Te}$.

Analysis of (60) shows that the parametric growth rate (and consequently the threshold) strongly depends on the wavelength of the excitations. If we increase $k\rho_e$ to be $k\rho_e \sim 1$, then $k_y \sim 10^2\ \mathrm{cm}^{-1}$ and, consequently, $k_y \gg k_{0x}$. Taking this into account from (62) we obtain

$$\frac{E_{0y}^{T}}{(4\pi n_e T_e)^{1/2}} + 15 k_y r_{De}\left(\frac{\Omega_e}{\omega_{pe}}\right)^2\left(\frac{k_y}{k_{0x}}\right)^2 \frac{V_{EB}^{(1)}}{L_y\Omega_e}, \quad k^2\rho_e^2 \sim 1. \quad (67)$$

For the above parameters and $V_{EB}^{(1)} \lesssim 10^{-2} V_{Te}$ ($k_y r_{De} \sim 1$), (67) gives $E_{0y}^{T} \gtrsim 50$ V/cm, which is significantly lower than the corresponding value in the long-wavelength region. In the extremely-short-wavelength region, the threshold is exponentially larger and is not of interest. Finally, let us note that such a low threshold exists for a very narrow bandwidth ($k^2\rho_e^2 \sim 1$) of the excited EBM.

In the second electron-cyclotron harmonic resonance layer, it is also possible to excite two EC waves with frequency spectrum given by (A10). In this case, in the coupling coefficient for the "ordinary" wave, the k_{0z} component of the driver pump is to be taken into account as well as k_z of the excited modes. Then

$$\mu_{H,2}^2 = \left\{\frac{e^2 k_y^2 E_{0y}^2}{9 m_e^2 \Omega_e^4}\left[1+\left(\frac{\Omega_e}{\omega_0}\right)^2\left(\frac{k_{0x}}{k_y}\right)^2\right] + \frac{e^2(k_z - k_{0z})^2 E_{0z}^2}{16 m_e^2 \Omega_e^4}\right\} \times\frac{(2k_z k_{0z} - k_{0x}^2 - k_{0z}^2)^2}{(k_y^2+k_z^2)[k_{0x}^2 + k_y^2 + (k_z - k_{0z})^2]}. \quad (68)$$

For the parametric growth rate we have

$$(\gamma + \gamma_e) = (\mu_{H,2}/2)\Omega_e(\omega_{pe}/\Omega_e)^2 \sin^2\theta. \quad (69)$$

Comparison of (60) and (69) reveals that the effectiveness of excitation of two obliquely propagating electron-cyclotron waves in the second electron-cyclotron resonance layer is somewhat lower (depending on θ) when compared to excitation of two EBM by the X-driver pump. However, in the case of launching of the predominantly O mode (20% goes to the X mode), the only possible parametric decay is the one described by (68) and (69). Another possibility for excitation is the simultaneous excitation of two upper-hybrid waves ($\Omega_e > \omega_{pe}$). In this case, in the long-wavelength region, results obtained for EBM are directly applicable [see (66)].

As saturation mechanism for parametrically excited EBM and obliquely propagating EC waves in the second ECHR layer, we shall invoke cascading processes described in Secs. II B 1 and II B 3. Utilizing expression (41) for the resultant turbulence electric field we obtain

$$E_{EB} \sim \left[\frac{1}{6}\frac{\Omega_e L_y}{V_{EB}^{(1)}}\left(\frac{\omega_{pe}}{\Omega_e}\right)^4 \frac{E_{0y}}{(4\pi n_e T_e)^{1/2}} \frac{k_{0x}^2 r_{De}}{k_y}\right]^{3/2} 2E_{0,THR} \quad (70)$$

in the long-wavelength region, and

$$E_{EB} \sim \left[6\times 10^{-2}\frac{\Omega_e L_y}{V_{EB}^{(1)}}\left(\frac{\omega_{pe}}{\Omega_e}\right)^2 \times\frac{E_{0y}}{(4\pi n_e T_e)^{1/2}} \frac{k_{0x}^2}{k_y^3 r_{De}}\right]^{3/2} 2E_{0,THR} \quad (71)$$

in the short-wavelength region ($k^2\rho_e^2 \sim 1$). In the case of weak driver pumps [$\gamma_0 \lesssim 5\,(L_y/V_{EB}^{(1)})$], from (70) we obtain $E_{EB} \gtrsim 1.5$ kV/cm for the saturated electric field of EBM. In the short-wavelength region, which is of more interest because of the lower threshold, we have $E_{EB} \sim 200$ V/cm. If this instability appears to be convective, then the nonlinearly absorbed energy is $(\gamma_0 L_y)/V_{EB}^{(1)}$ times [see (53)] larger than in the case of absolute instabilities. For the convective case, the nonlinearly absorbed power density reads:

$$Q^{conv} = \frac{1}{8}\frac{\mu_H^4 L_y^3}{(V_{EB}^{(1)})^3}\frac{\omega_{pe}^8}{\Omega_e^4} W_{0,THR}, \quad k^2\rho_e^2 \ll 1, \quad (72)$$

and in the short-wavelength region,

$$Q^{\rm conv} = 2\frac{\mu_H^4 L_y^3}{(V_{\rm EB}^{(1)})^3}\frac{k^8 r_{De}^8 \Omega_e^4 A_1^4(k_\perp^2\rho_e^2)}{[1+k^2 r_{De}^2 - A_0(k_\perp^2\rho_e^2)]^8} W_{0,\rm THR},$$
$$k^2\rho_e^2 \sim 1. \tag{73}$$

Let us now study excitation of the EC harmonic waves coupled to some of the low-frequency modes. The coupling coefficient in this case, for the same geometry used in obtaining (58), has the form

$$\mu_L^2 = \frac{e^2 k_y^2 E_{0y}^2}{m_e^2[\phi(l)]^2}\left[1+\left(\frac{\Omega_e}{\omega_0}\right)^2\left(\frac{k_{0x}}{k_y}\right)^2\right] \times\frac{k_y^2+k_z^2}{4[k_{0x}^2+k_y^2+(k_z-k_{0z})^2]}[1+\mathrm{Re}\,\chi_e(\omega_1\mathbf{k})]^2. \tag{74}$$

For the parametric growth rate we obtain

$$(\gamma+\gamma_{\rm EB}^{(l)})(\gamma+\gamma_L) = \mu_L^2(l\Omega_e/\omega_{pe}^2)k^2\rho_e^2 \times\left[\sum_{l=-\infty}^{+\infty}\frac{l^2 A_l(k^2\rho_e^2)}{(\omega-l\Omega_e)^2}\left(\frac{\partial\,\mathrm{Re}\,\epsilon_L}{\partial\omega}\right)_{\substack{\omega=\omega_L\\ \mathbf{k}=\mathbf{k}_L}}\right]^{-1}. \tag{75}$$

In (75), ϵ_L is the low-frequency dielectric permittivity corresponding to the relevant low-frequency mode and $\omega \equiv -\omega_{\rm EB}^{(l)} = \omega_L - \omega_0$. Expression (75) can be applied to EBT plasma if $l=2$, which corresponds to the excitation of the EBM with frequency $\omega_{\rm EB}^{(2)} \sim 2\Omega_e$ coupled to some of the low-frequency modes in the second electron-cyclotron harmonic layer. For low-frequency modes we shall study the lower-hybrid wave,

$$\mathrm{Re}\,\epsilon_{\rm LH} \sim 1 + \frac{\omega_{pe}^2}{\Omega_e^2} - \frac{\omega_{pi}^2}{\omega^2},$$

the ion-acoustic wave,

$$\mathrm{Re}\,\epsilon_{IA} \sim 1 + (kr_{De})^{-2} - \omega_{pi}^2/(\omega^2-\Omega_i^2),$$

and the ion-Bernstein wave,

$$\mathrm{Re}\,\epsilon_{\rm IB} \sim 1 + (kr_{De})^{-2} - \frac{\omega_{pi}^2}{\omega}\sum_{l=-\infty}^{+\infty}\frac{l^2 A_l(k^2\rho_i^2)}{k^2\rho_i^2(\omega-l\Omega_i)}.$$

From (74) it is evident that the finite wavelength of a driver pump for this type of parametric instability does not play a crucial role as in (58). Furthermore, for this excitation the approximation of a dipole driver pump ($k_0 \sim 0$) is valid. For the excitation of the lower-hybrid wave, the parametric growth rate is given by ($k^2\rho_e^2 \ll 1$)

$$(\gamma+\gamma_{\rm EB}^{(2)})(\gamma+\gamma_{\rm LH}) = \frac{\mu_{\rm LH}^2}{8}\frac{\omega_{\rm LH}\Omega_e^3}{\omega_{pe}^2}\frac{(k^2\rho_e^2)^3}{k^4 r_{De}^4}. \tag{76}$$

Here $\mu_{\rm LH}$ is μ_L for $1+\chi_e(\omega,\mathbf{k}) \sim 1$. In (76), in the case of excitation of well-defined LHW, we have $\gamma > \gamma_{\rm EB}^{(2)}, \omega_{\rm LH}$, and in the case of excitation of heavily damped (quasimode) LHW we have $\gamma \ll \gamma_{\rm LH} \lesssim \omega_{\rm LH}$. Here $\omega_{\rm LH}$ is the lower-hybrid frequency given by

$$\omega_{\rm LH} = \omega_{pi}[1+(\omega_{pe}/\Omega_e)^2]^{-1/2},$$

where ω_{pi} is the ion-plasma frequency. Repeating the procedure for finding a threshold, the following expression is obtained:

$$\frac{(E_{0y}^T)^2}{4\pi n_e T_e} \sim \frac{288}{\omega_{\rm LH}\Omega_e}\left(\frac{\Omega_e}{\omega_{pe}}\right)^2\frac{(k_y r_{De})^2}{(k\rho_e)^6}\frac{V_{\rm EB}^{(2)}V_{\rm LH}}{L_y^2}, \quad k^2\rho_e^2 \ll 1. \tag{77}$$

Here $V_{\rm LH}$ is the group velocity of LHW given by (for the case of "cold" LHW)

$$V_{\rm LH} = \omega_{\rm LH}\left(\frac{k_z}{k^2}\right)\frac{m_i}{m_e}\left\{-\frac{k_x k_z}{k^2}, \quad -\frac{k_y k_z}{k^2}, \quad 1\right\},$$

and $\gamma_{\rm LH}$ is the corresponding linear damping rate. Substituting typical values for EBT-S parameters for the case of well-defined LHW ($\gamma_{\rm LH} \ll V_{\rm LH}/L_y$), the threshold value of the electric field $E_{0y}^T \gtrsim 600$ V/cm is obtained ($V_{\rm EB}^{(2)} \gtrsim 5\times 10^{-2} V_{Te}$, $V_{\rm LH} \gtrsim 10^{-2} V_{Te}$). It is easy to prove that for the same parameters [see (75)], the threshold value for the excitation of ion-acoustic quasimode (in order to satisfy selection rules, ion-acoustic waves propagate nearly perpendicularly and, consequently, are heavily damped) is three times larger, and in the case of ion-Bernstein harmonics twice (or less depending on harmonic number l) as large as the above value.

For shorter wavelengths, instead of (76) we have

$$(\gamma+\gamma_{\rm EB}^{(2)})(\gamma+\gamma_{\rm LH}) = \mu_{\rm LH}^2\Omega_e\omega_{\rm LH}\frac{k^2 r_{De}^2 A_2(k_\perp^2\rho_e^2)}{[1+k^2 r_{De}^2 - A_0(k_\perp^2\rho_e^2)]^2}. \tag{78}$$

It is easy to see that the growth rate given by (78) for $k^2\rho_e^2 \sim 1$ is nearly twice as large as the value obtained by (76) for the same excess over threshold (E_{0y}/E_{0y}^T). A significant decrease in the threshold could be reached in the $k^2\rho_e^2 \sim 1$ region because of the extremely small group velocity $V_{\rm EB}^{(2)}$ [see (65)]. It is to be noted that dissipative threshold cannot be in competition with the inhomogeneous one because of the negligible collisional damping rate of EBM for $l>1$ [see (A7)]. For the threshold value in the $k^2\rho_e^2 \sim 1$ region in the case of excitation of well-defined LH modes, we obtain

$$\frac{(E_{0y}^T)^2}{4\pi n_e T_e} \sim 72\left(\frac{\Omega_e}{\omega_{pe}}\right)^4\frac{[1+k^2 r_{De}^2 - A_0(k_\perp^2\rho_e^2)]^2}{(k_y r_{De})^2(kr_{De})^2 A_1(k_\perp^2\rho_e^2)} \times\frac{V_{\rm EB}^{(2)}V_{\rm LH}}{L_y^2\omega_{\rm EB}^{(2)}\omega_{\rm LH}}. \tag{79}$$

The threshold value for the excitation of the lower-hybrid quasimode could be obtained from (79) by the substitution $V_{\rm LH}/L_y\omega_{\rm LH} \to \gamma_{\rm LH}/\omega_{\rm LH} \lesssim 1$. In the spatial regions where excitation of a well-defined LHW is possible, depending on the mismatching quantity $\Delta = \omega_0 - 2\Omega_e(y)$, from (79) for EBT-S parameters and for $k^2\rho_e^2 \sim 1$, $V_{\rm EB}^{(2)} \sim 10^{-3} V_{Te}$, we obtain values for E_{0y}^T around 60 V/cm.

The saturation level of the excited second harmonic EBM could again be thus invoking cascadings. It is to be noted that primary excited second harmonic EBM can further decay into other SHEBM coupled to some of the low-frequency modes in the long-wavelength region or into two principal harmonic EBM in the short-wavelength region, $k^2\rho_e^2 \gg 1$. The latter case, however, is not of interest because of the relatively high thresholds for primary excitations. Utilizing (40), we have

$$E_{\rm EB}^2 \sim \frac{\mu_{\rm LH}^3 L_y^2}{\gamma_{\rm LH}(V_{\rm EB}^{(2)})^2\sqrt{2}}\frac{k^3 r_{De}^3(\omega_{\rm LH}\Omega_e)^{3/2}A_2^{3/2}(k_\perp^2\rho_e^2)}{[1+k^2 r_{De}^2 - A_0(k_\perp^2\rho_e^2)]^3}(E_{0y}^T)^2. \tag{80}$$

For the same excess over threshold (E_{0y}/E_{0y}^T) ($\gamma \lesssim 5\, V_{\rm EB}/L_y$,

$\gamma \gtrsim \gamma_{LH}$) in the long- and short-wavelength ($k^2\rho_e^2 \sim 1$) region from (80), we obtain 3 kV/cm and 300 V/cm, respectively. The electric field E_{EB} given by (80) is (γ_0/γ_{LH}) times larger [where $\gamma_0 > \gamma_{LH}$] than the corresponding value in the case of excitation of LHQM ($\gamma_0 < \gamma_{LH}$) [compare (38) and (40)]. By use of the expression (53) for the nonlinearly absorbed power density we obtain

$$Q^{\text{conv}} = \frac{\mu_{LH}^4 L_y}{\gamma_{LH}^2 V_{EB}^{(2)}} \frac{(\omega_{LH}\Omega_e)^2 (kr_{De})^4 A_2^2(k_\perp^2\rho_e^2)}{[1 + k^2 r_{De}^2 - A_0(k_\perp^2\rho_e^2)]^4} W_{0,THR}. \tag{81}$$

Finally, let us consider excitation in the principal electron-cyclotron resonance layer (see Fig. 1). As seen from Fig. 1, this layer is accessible for the case of axial launching (Fig. 4). Here we shall assume that the driver pump propagates along the z axis with the electric field along the y axis. Then the coupling coefficient reads (resonant excitation)

$$\mu_1^2 = \frac{e^2 k_y^2 E_{0y}^2 (k_y^2 + k_z^2)}{16[k_y^2 + (k_z - k_{0z})^2] m_e^2 \Omega_e^4} \times \frac{[1 + k^2 r_{De}^2 - A_0(k_\perp^2\rho_e^2)]^2}{A_1^2(k_\perp^2\rho_e^2)} [1 + \text{Re}\,\chi_e(\omega,\mathbf{k})]^2. \tag{82}$$

For the parametric growth rate and threshold in the case of excitation of LHW, we obtain

$$(\gamma + \gamma_{EB}^{(1)})(\gamma + \gamma_{LH}) = \frac{\mu_1^2}{2} \frac{k^2 r_{De}^2 \Omega_e \omega_{LH} A_1(k_\perp^2\rho_e^2)}{[1 + k^2 r_{De}^2 - A_0(k_\perp^2\rho_e^2)]^2}, \tag{83}$$

$$\frac{(E_{0y}^T)^2}{4\pi n_e T_e} = 8\left(\frac{\Omega_e}{\omega_{pe}}\right)^4 \frac{A_1(k_\perp^2\rho_e^2)}{(k_y r_{De})^2 (kr_{De})^2} \frac{V_{EB}^{(1)} V_{LH}}{L_y^2 \Omega_e \omega_{LH}}. \tag{84}$$

In the short-wavelength region $k^2\rho_e^2 \sim 1$, from (84) E_{0y}^T is approximately 40 V/cm ($T_e \sim 500$ eV, $n_e \sim 2\times 10^{12}$ cm^{-3}, and $V_{EB}^{(1)} \sim 10^{-2} V_{Te}$). In the long-wavelength region ($k^2\rho_e^2 \ll 1$), the threshold is greater by an order of magnitude. For the saturated electric field we have

$$E_{EB}^2 = \frac{\mu_1^3 L_y^2}{(V_{EB}^{(1)})^2 \gamma_{LH}} \left(\frac{\Omega_e \omega_{LH}}{2}\right)^{3/2} \times \frac{k^3 r_{De}^3 A_1^{3/2}(k_\perp^2\rho_e^2)}{[1 + k^2 r_{De}^2 - A_0(k_\perp^2\rho_e^2)]^3} (E_{0y}^T)^2. \tag{85}$$

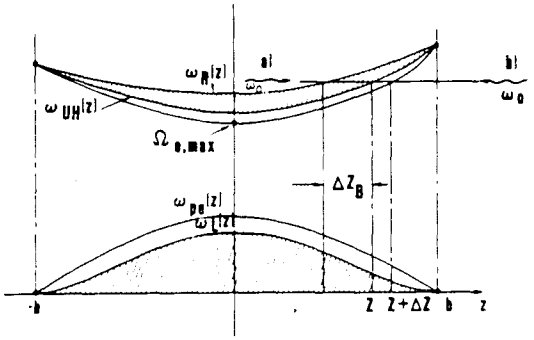

FIG. 4. Axial launching of the X and O mode. Notation is the same as in Fig. 2(a). Case (a) corresponds to reflected waves from the wall at the inner side of EBT. Case (b) denotes axial launching from the high-field sides of EBT.

In the near-threshold regime for $k^2\rho_e^2 \sim 1$, (85) gives $E_{EB} \gtrsim 200$ V/cm.

Another possibility of parametric excitation in the principal harmonic layer is excitation of the obliquely propagating EC wave. For both X and O modes, the driver pump threshold is somewhat higher than the corresponding one for the excitation of the EBM. In the case of the O-driver pump launching, excitation of EBM does not take place, and the only possible decay is $\omega_0 \rightarrow \text{OEC} + L$, to an obliquely propagating EC wave and a low-frequency mode.

IV. UPPER-HYBRID RESONANCE

Reflected electromagnetic waves from the wall of the EBT (inner side, see Fig. 1) can reach an upper-hybrid resonance layer. This process is possible because of the very small distance between the ω_R layer and the ω_{UH} layer given by $\Delta Z_B = L_B[\omega_R(z)/\Omega_e(z) - 1]$, $L_B = [(1/B)(dB/dz)]^{-1}$, which is comparable to the length of evanescence $\Delta Z_e = [c/\Omega_e(z)L_{N,z}]^{2/3} L_{N,z}$, $L_{N,z} = [(1/n)(dn/dz)]^{-1}$. Accordingly, we shall assume that significant WKB enhancement of the pump electric field takes place in the UH resonance layer, where the transverse pump wave is linearly converted into longitudinal UH or EBM waves.[38,39] Consequently, in our calculations we shall include the WKB process in the component E_{0x} (actually this is the electric field of the linearly converted mode) which is typically $E_{0x}/E_{0y} \gtrsim 5$. Parametric processes in the upper-hybrid resonance layer can also be induced by axial launching from the high-field side of the X-mode driver pump. In both cases, propagation of EBM or UH waves is along the X axis. The coupling coefficient has the form

$$\mu_{L,UH}^2 = \frac{E_{0x}^2}{4\pi n_e T_e}(k_x r_{De})^2 \left[1 + \left(\frac{\Omega_e}{\omega_0}\right)^2 \left(\frac{E_{0y}}{E_{0x}}\right)^2\right] \times [1 + \text{Re}\,\chi_e(\omega,\mathbf{k})]^2. \tag{86}$$

In (86) the driver pump is treated in the dipole approximation. For the parametric growth rate we have

$$(\gamma + \gamma_{UH})(\gamma + \gamma_{LH}) = \mu_{L,UH}^2 (\omega_{LH}\omega_{UH})(\omega_{pe}/\omega_{UH})^2/4. \tag{87}$$

For the threshold value (convective threshold) we obtained

$$\frac{(E_{0x}^T)^2}{4\pi n_e T_e} \sim \left(\frac{\omega_{UH}}{\Omega_e}\right)^2 \frac{1}{(k_x\rho_e)^2} \frac{(\gamma_{UH} V_{LH} + \gamma_{LH} V_{UH})^2}{\omega_{UH}\omega_{LH} V_{LH} V_{UH}}, \quad (k_x\rho_e)^2 \ll 1. \tag{88}$$

From (88) for EBT-S and for $(k_x\rho_e)^2 \sim 10^{-1}$, $E_{0x}^T \gtrsim 400$ V/cm. Taking into account WKB enhancement, we obtain $E_{0y}^T \sim 70$ V/cm.

For the saturated electric field of upper-hybrid wave, we have ($\gamma_0 > \gamma_{LH}$)

$$E_{UH}^2 \sim \frac{\mu_{L,UH}^3}{8\gamma_{UH}^2\gamma_{LH}} \omega_{pe}^3 \left(\frac{\omega_{LH}}{\omega_{UH}}\right)^{3/2} (E_{0,x}^T)^2, \tag{89}$$

and in the case of LHQM ($\gamma_0 \ll \gamma_{LH}$),

$$E_{UH}^2 \sim \frac{\mu_{L,UH}^4}{16\gamma_{LH}^2\gamma_{UH}^2} \omega_{pe}^4 \left(\frac{\omega_{LH}}{\omega_{UH}}\right)^2 (E_{0,x}^T)^2. \tag{90}$$

The nonlinearly absorbed power density is ($\gamma_0 > \gamma_{LH}$)

$$Q^{\text{conv}} = \frac{\mu^4_{L,\text{UH}}}{16\gamma^2_{\text{LH}}\gamma_{\text{UH}}}\omega^4_{pe}\left(\frac{\omega_{\text{LH}}}{\omega_{\text{UH}}}\right)^2 W_{0,\text{THR}}. \quad (91)$$

Here γ_{UH} is the linear damping rate of the upper-hybrid wave [see (A12)].

Finally, one more possibility of parametric excitation in the principal harmonic resonance layer is the case of O-mode launching in the axial (from the high-field side) or radial (from the low-field side) directions (see Sec. III).

V. LOWER-HYBRID RESONANCE

In the past decade, a comprehensive linear theory of parametric instabilities in the lower-hybrid frequency range (LHFR) has been developed.[20,40] In contrast to a large number of papers dealing with the linear theory of parametric instabilities, only a few papers treated saturation processes.[36,40] In this section we shall give a power balance treatment of saturation processes (see Secs. II B 1 and II B 3) for the EBT environment.

We consider mode–mode coupling processes along the propagation cone of a slow wave[41] in EBT plasma (see Fig. 5). The geometry of interaction is defined as follows: In the vacuum we assume $\mathbf{E}_0 = \{E_{0x},0,E_{0z}\}$, $E_{0x}/E_{0z} \ll 1$, and for the driver pump wave vector $\mathbf{k}_0 = \{k_{0x},0,k_{0z}\}$ with $k_{0z}/k_{0x} \ll 1$, nearly perpendicular incidence. In the case of a slow-wave launched (the other possibility is launching of a fast-whistler wave)[42] from a plasma boundary, $n_z = ck_{0z}/\omega_0 > 2$, the electric field in a plasma (shaded area in Fig. 5) is quasielectrostatic with $k_z/k_\perp \sim k_{0z}/k_{0\perp} \sim E_{0z}/E_{0\perp} \ll 1$, where $\perp$ denotes quantities normal to $\mathbf{B}_0$.

For the above assumed propagation of a driver pump in the x-z plane, using (6) and (7) for the coupling coefficient, we obtain (ion dynamics are neglected)

$$\mu^2_L = \frac{e^2k^2\,\text{Re}\,\chi_i(\omega,\mathbf{k})[1+\text{Re}\,\chi_e(\omega,\mathbf{k})]}{4m_e^2\omega_0^4(\mathbf{k}-\mathbf{k}_0)^2}\left[\left((k_z-k_{0z})E_{0z} + (k_x-k_{0x})E_{0x}\frac{\omega_0^2}{\omega_0^2-\Omega_e^2}\right)^2 + k_y^2E_{0x}^2\frac{\omega_0^2\Omega_e^2}{(\omega_0^2-\Omega_e^2)^2}\right]. \quad (92)$$

This is the general coupling coefficient taking into account parallel, polarization, and $\mathbf{E}_0\times\mathbf{B}_0$ drift coupling. In what follows, the region of interaction will be divided into several zones (see Fig. 6) to distinguish between E_{0z} and $\mathbf{E}_0\times\mathbf{B}_0$ dominant coupling and excitation of Gould–Trivelpiece (G–T) modes, $(k_z/k)^2 m_i/m_e \ll 1$, and lower-hybrid waves that appear to be the limiting case of G–T modes when $(k_z/k)^2 m_i/m_e \lesssim 1$. We call the zone where G–T modes could be excited (zone II in Fig. 6) the edge plasma zone and the zone with effective excitation of LHW the lower-hybrid wave zone.

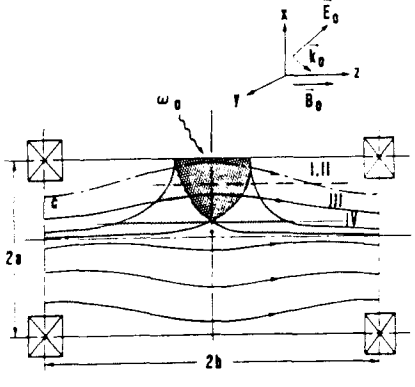

FIG. 5. Resonance cone propagation of lower-hybrid wave in EBT (shaded area) and geometry of the magnetic field and driver pump in the vacuum. Zones I, II, III, and IV are explained in Fig. 3. Here $2b$ is the length and $2a$ is the width of one mirror section.

A. Nonlinear processes near the edge of EBT plasma

As seen from (92) the ratio between E_{0z} drift and $\mathbf{E}_0\times\mathbf{B}_0$ electron rf drift coupling is ($k_z \gg k_{0z}$): $(E_{0z}/E_{0x})^2(k_z/k_y)^2(\Omega_e/\omega_0)^2$. For LHW $(k_z/k_y)\sim(m_e/m_i)^{1/2}$ and for typical driver frequency, e.g., the $f_0 \sim 300$ MHz used in linear heating simulation[42] of EBT, the E_{0z} coupling dominates in electron density regions where $n_e(\text{cm}^{-3}) \lesssim 0.5\Omega_e(s^{-1})$ (Ω_e is the electron-cyclotron frequency at the edge of EBT). For $B_0 \sim 0.1$–0.3 T at the edge we have $n_e \lesssim (1$–$4)\times 10^{10}$ cm^{-3} (see Fig. 5, zone I). In this region, excitation of Gould–Trivelpiece modes with a frequency spectrum of

$$\omega = \omega_{pe}(r)(k_z/k)(1+\tfrac{1}{2}k^2r_{De}^2), \quad k^2r_{De}^2 < 1, \quad (93)$$

can take place. The corresponding real part of the dielectric permittivities is

$$\text{Re}\,\epsilon(\omega,\mathbf{k}) = 1 - \omega_{pe}^2\cos\theta/\omega^2, \qquad \cos\theta \equiv k_z/k. \quad (94)$$

In (93), $\omega_{pe}(r)$ is the local electron plasma frequency. It is easy to see from (93) that for propagation $k_z/k \lesssim (m_e/m_i)^{1/2}$ a G–T mode transforms into a LHW $\omega \sim \omega_{pi}(r)$. The density threshold for excitation of G–T modes could be obtained from $\omega_0 \sim \omega_{pi}(0) \sim \omega_{pe}(r)\cos\theta + \omega_L$ (ω_L frequency of some low-frequency mode). For G–T modes with $\cos^2\theta\,(m_i/m_e) \gtrsim 10$, we have a density threshold $n_e \lesssim 3.6\times 10^{11}$ cm^{-3} (Fig. 6, zone II). Similarly, the density threshold for excitation of LHW ($\cos^2\theta \lesssim m_e/m_i$) in deuterium plasma is $n_e \lesssim 9\times 10^{12}$ cm^{-3}. Accordingly, in zones III and IV in Fig. 5, it is potentially (if the electric field is strong enough) possible to excite LHW.

In zone I, the G–T mode wave vector is $\mathbf{k} = \{k_x,0,k_z\}$. Here $k_y = 0$ because the $\mathbf{E}_0\times\mathbf{B}_0$ drift is negligible and k_x,k_z are consequences of charge separation along E_{0x},E_{0z}, respectively. Now, from (92) we have

$$\mu^2_{L\,\text{I}} = \frac{(1+\text{Re}\,\chi_e)^2(kr_{De})^2}{16(\mathbf{k}-\mathbf{k}_0)^2\pi n_eT_e}\left(\frac{\omega_{pe}}{\omega_0}\right)^4 \times\left[(k_z-k_{0z})E_{0z} - (k_x-k_{0x})E_{0x}(\omega_0^2/\Omega_e^2)\right]^2. \quad (95)$$

From (95) it is evident that even in the case of a strong E_{0x} component, coupling caused by E_{0z} is dominant. In the region with $n_e \lesssim 4\times 10^{10}$ cm^{-3}, the electron plasma frequency is $\omega_{pe} \lesssim 10^{10}$ sec^{-1} so that a driver pump with frequency $f_0 \sim 300$ MHz can excite G–T modes with $\cos\theta \gtrsim 2\times 10^{-1}$. Excitation of Langmuir waves ($\cos\theta \sim 1$) is possible in a region of $n_e \lesssim 5\times 10^8$ cm^{-3}. Deposition of the driver pump energy in the latter case is negligible because of the extremely small plasma frequency. This case is equivalent to $E_{0x} \sim 0$ (and consequently $k_x \sim 0$), which is appropriate at the plasma edge where density gradient along x is negligible. In

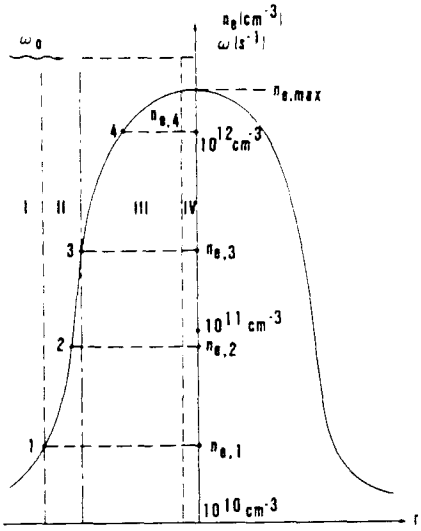

FIG. 6. Radial profile of plasma density, n_e, at the midplane ($z=0$) for EBT-S. The frequency of the driver pump is $f_0 \sim 300$ MHz, and $n_{e,max} = 2\times 10^{12}$ cm^{-3}. Zone I represents a region of dominant E_{0z} radio-frequency electron drift coupling, and zones II, III, and IV of dominant $\mathbf{E}_0\times\mathbf{B}_0$ radio frequency electron drift coupling. The density threshold for $\mathbf{E}_0\times\mathbf{B}_0$ coupling is $n_{e,1}\sim 4\times 10^{10}$ cm^{-3}. Zone II, including zone I, represents a region of effective excitation of Gould–Trivelpiece (G–T) modes, and zones III and IV are zones of excitation of lower-hybrid waves. Conditionally, in this paper, zones I and II are called the plasma edge zones. The maximum density for excitation of G–T modes coupled to an ion-cyclotron wave is obtained for $\cos^2\theta(m_i/m_e)\gtrsim 10$ and amounts to a value of $n_e = 3.6\times 10^{11}$ cm^{-3}. Zone IV is the region of strong linear conversion processes and is not considered in this paper. A plasma density where $\omega_0\sim 2\omega_{pe}(r)\cos\theta$, $\cos^2\theta(m_i/m_e)\gtrsim 10$ is given by $n_{e,2}\sim 9\times 10^{10}$ cm^{-3} and the density at which excitation of two lower-hybrid waves [$\cos^2\theta(m_i/m_e)\lesssim 1$] takes place is given by $n_{e,4}\lesssim 10^{12}$ cm^{-3}.

somewhat deeper regions, E_{0x} becomes significant because of the density gradient along x (see Fig. 5) and the k_x component of the excited mode is appreciable.

In the region between points 1 and 2 (Fig. 6), coupling caused by the $\mathbf{E}_0\times\mathbf{B}_0$ electron rf drift becomes dominant and the coupling coefficient, obtained from (92), has the form

$$\mu_{L,2}^2 = \frac{k_y^2}{4}\left[1+\left(\frac{k_z}{k_y}\right)^2\right]\frac{(1+\mathrm{Re}\,\chi_e)^2}{k_{0x}^2+k_{0y}^2-(k_z-k_{0z})^2} \times\frac{E_{0x}^2}{4\pi n_e T_e}(k_y r_{De})^2\left(\frac{m_i}{m_e}\right)\left(\frac{\omega_{pe}}{\Omega_e}\right)^2 \times\left[1+\left(\frac{\omega_0}{\Omega_e}\right)^2\left(\frac{k_{0x}}{k_y}\right)^2\right]. \quad (96)$$

In (96), k_y is a consequence of $\mathbf{E}_0\times\mathbf{B}_0$ coupling and k_z of the E_{0z} component. Accordingly, in this case, propagation of G–T modes is in the y-z plane.

In the region left of point 3 (Fig. 6) where $\omega_0\sim\omega_{pi}(0)\gtrsim 2\omega_{pe}(r)\cos\theta$, it is possible to excite simultaneously two G–T modes. If E_{0z} coupling is dominant, they will propagate opposite ($\mathbf{k}>\mathbf{k}_0$) in the x-z plane and in the case of dominant $\mathbf{E}_0\times\mathbf{B}_0$ coupling, they will propagate in the y-z plane. The corresponding coupling coefficients could be obtained from (7) and (8) in the form

$$\mu_{H,1}^2 = \frac{e^2}{m_e^2\omega_0^4}\frac{[(k_z-k_{0z})E_{0z}-(k_x-k_{0x})E_{0x}(\omega_0^2/\Omega_e^2)]^2}{(k_x^2+k_z^2)[(k_x-k_{0x})^2+(k_z-k_{0z})^2]} \times[k_{0x}(2k_x-k_{0x})+k_{0z}(2k_z-k_{0z})]^2, \quad (97)$$

in the case of dominant E_{0z} coupling, and

$$\mu_{H,2}^2 = \frac{e^2k_y^2E_{0x}^2}{m_e^2\omega_0^2\Omega_e^2}\frac{[k_{0x}^2+k_{0z}(2k_z-k_{0z})]^2}{(k_y^2+k_z^2)[k_{0x}^2+k_y^2+(k_z-k_{0z})^2]}, \quad (98)$$

in the case of dominant $\mathbf{E}_0\times\mathbf{B}_0$ coupling or, in other words, when propagation of G–T modes is in the y-z plane.

Let us first consider the excitation of a G–T mode coupled to ion-cyclotron waves. For the parametric growth rate, we obtain from (2):

$$(\gamma+\gamma_{G\text{-}T})(\gamma+\gamma_{IC}^{(n)}) = (\mu^2/2)(\omega_{pe}\,\Omega_i\cos\theta) \times\frac{k^2r_{De}^2}{(1+k^2r_{De}^2)^2}\frac{T_e}{T_i}nA_n(k_\perp^2\rho_i^2). \quad (99)$$

Here $\gamma_{G\text{-}T}$ and $\gamma_{IC}^{(n)}$ are the linear damping rates of G–T modes and ion-cyclotron waves (see Appendix). In (99) coupling of the modes can be through $E_{0z}(\mu=\mu_{L,1})$ or the $(\mathbf{E}_0\times\mathbf{B}_0)(\mu\equiv\mu_{L,2})$ coupling mechanism. Maximizing the growth rate with respect to $k_\perp\rho_i$ gives $k_\perp\rho_i\sim 1.2$. A slight decrease in growth rate with increase of n is also seen from (99).

In region 1 (see Fig. 6), we have dominant E_{0z} coupling and, consequently, propagation of the G–T mode will be in the x-z plane, so that $\mathbf{k}_{G\text{-}T}=\{k_x,0,k_z\}$ with $k_z/k_x\ll 1$. Further, in this type of excitation, as seen in (6) the dipole approximation for the driver pump is valid so that for the threshold value of the electric field we obtain

$$\frac{E_{0z,T}^2}{4\pi n_e T_e} = \left(\frac{\omega_0}{\omega_{pe}}\right)^4\frac{1}{(k_z r_{De})^2}\frac{8}{(1+\mathrm{Re}\,\chi_e)^2\omega_{pe}\cos\theta\Omega_i} \times\frac{(1+k^2r_{De}^2)^2}{k^2r_{De}^2}\frac{T_i}{T_e}\frac{1}{nA_n(k_\perp^2\rho_i^2)}\frac{V_{G\text{-}T}V_{IC}^{(n)}}{L^2}, \quad (100)$$

where $V_{G\text{-}T}$ and $V_{IC}^{(n)}$ are group velocities of G–T and ion-cyclotron waves, given by

$$\mathbf{V}_{G\text{-}T} = \{-\omega_{pe}k_zk_x/k^3,0,\omega_{pe}k_x^2/k^3\}, \quad k^2 = k_x^2+k_z^2, \quad (101)$$

and $\mathbf{V}_{IC}^{(n)} = \partial\omega/\partial\mathbf{k}$, where ω takes the form (A17) in the case of excitation of ion-Bernstein modes and form (A18) in the case of excitation of ion-cyclotron waves. Also, in the case of excitation of IB modes, $\mathrm{Re}\,\chi_e = -(1/n^2)(\omega_{pe}/\Omega_i)^2\cos^2\theta$, $\cos^2\theta(m_i/m_e)\lesssim 1$ [see (A14)], and in the case of excitation of ion-cyclotron waves $\mathrm{Re}\,\chi_e=(kr_{De})^{-2}$ [see (A15)]. As seen from (101), the x component of the group velocity is dominant; accordingly in (100), $V_{G\text{-}T}$ and V_{IC} represent the x component of group velocities. In (100), L is a wavenumber mismatching quantity which in the case of 2π foldings is given by[43] $L=[1/(\partial\Delta k_i/\partial x_i)]^{1/2}$ where $\Delta\mathbf{k}=\mathbf{k}_0-\mathbf{k}_1-\mathbf{k}_2$ and i denotes the relevant axis.

In zone II (see Fig. 6), G–T modes coupled to ion-cyclotron waves are excited by the $\mathbf{E}_0\times\mathbf{B}_0$ coupling mechanism. In this case, G–T modes propagate in the y-z plane. Conse-

quently, $\mathbf{k}_{G\text{-}T}=\{0,k_y,k_z\}$, $k_y/k_z \gg 1$. For the threshold value we have

$$\frac{E_{0x}^2}{4\pi n_e T_e} = \frac{8}{(1+\mathrm{Re}\,\chi_e)^2}\frac{1}{(k_y r_{De})^2}\left(\frac{\omega_{pi}}{\omega_{pe}}\right)^2\left(\frac{\Omega_e}{\omega_{pe}}\right)^2\frac{(1+k^2 r_{De}^2)^2}{k^2 r_{De}^2} \times\frac{T_i}{T_e}\frac{1}{nA_n(k_\perp^2\rho_i^2)}\frac{1}{\omega_{pe}\cos\theta\Omega_i}\frac{V_{G\text{-}T}V_{IC}}{L^2}, \quad (102)$$

where

$$\mathbf{V}_{G\text{-}T}=\{0,-\omega_{pe}k_y k_z/k^3,\omega_{pe}(k_y^2/k^3)\}, \qquad k^2=k_y^2+k_z^2. \quad (103)$$

In this case, propagation of the driver pump is in the x-z plane, while convection of excited waves is in the y-z plane, but mainly along the z axis [see (103)].

Point 2 in Fig. 6 denotes the surface at which the driver pump frequency is twice the local G–T mode frequency for propagation $\cos^2\theta\,(m_i/m_e)\gtrsim 10$. Consequently, to the left of point 2 it is possible to excite two G–T modes in region I by the E_{0z} coupling mechanism and in region II by the $\mathbf{E}_0\times\mathbf{B}_0$ coupling mechanism.

The parametric growth rate for the excitation of two G–T modes has the form

$$\gamma+\gamma_{G\text{-}T}=\tfrac{1}{2}\mu\omega_{pe}\cos\theta. \quad (104)$$

In the case of dominant E_{0z} coupling, G–T modes propagate in the x-z plane nearly opposite ($|\mathbf{k}_{G\text{-}T}|\gg|\mathbf{k}_0|$) from that in the short-wavelength region. For the electric field threshold value we obtain

$$\frac{E_{0z,T}^2}{4\pi n_e T_e}=\frac{1}{(k_z r_{De})^2}\left(\frac{\omega_0}{\omega_{pe}}\right)^4\left(\frac{k}{k_{0x}}\right)^2\frac{1}{\omega_{pe}^2\cos^2\theta}\frac{V_{G\text{-}T}^2}{L^2}. \quad (105)$$

In (105) it was assumed that $k_x \ll k_z$, and for the group velocity the z component has to be taken [see (101)].

In the case of dominant $\mathbf{E}_0\times\mathbf{B}_0$ coupling, two G–T modes can be excited in the region between points 1 and 2 (see Fig. 6). Waves propagate nearly opposite in the y-z plane. For the electric field threshold value we have

$$\frac{E_{0x,T}^2}{4\pi n_e T_e}=\frac{4}{(k_y r_{De})^2}\left(\frac{\omega_0}{\omega_{pe}}\right)^2\left(\frac{\Omega_e}{\omega_{pe}}\right)^2\left(\frac{k_y}{k_{0x}}\right)^4 \times\frac{1}{\omega_{pe}^2\cos^2\theta}\frac{V_{G\text{-}T}^2}{L^2}. \quad (106)$$

In both (105) and (106) we have assumed relatively shorter wavelengths ($|\mathbf{k}|>|\mathbf{k}_0|$) of the excited waves, which give higher thresholds but the case is more interesting from the aspect of plasma heating.

B. Nonlinear processes in the interior of EBT plasmas

Let us now consider region III (Fig. 6) where excitation of a lower-hybrid wave coupled to some low-frequency mode or two-coupled lower-hybrid waves can take place. If a LHW coupled to the ion-cyclotron harmonic wave is excited, the parametric growth rate for resonant excitation has the form (note that in zone III only $\mathbf{E}_0\times\mathbf{B}_0$ coupling is possible)

$$(\gamma+\gamma_{LH})(\gamma+\gamma_{IC}^{(nl)}) = \frac{E_{0x}^2}{4\pi n_e T_e}\frac{[1+\mathrm{Re}\,\chi_e(\omega,\mathbf{k})]^2}{8}(k_y r_{De})^2\left(\frac{\omega_{pe}}{\omega_0}\right)^2 \times\left(\frac{\omega_{pe}}{\Omega_e}\right)^2\omega_{LH}\Omega_i\frac{k^2 r_{De}^2}{(1+k^2 r_{De}^2)^2}\frac{T_e}{T_i}nA_n(k_\perp^2\rho_i^2). \quad (107)$$

Taking appropriate values (see Appendix) for $\mathrm{Re}\,\chi_e(\omega,\mathbf{k})$, (107) describes the excitation LHW + ICW or LHW + IBM. Furthermore, in order to satisfy selection rules $\omega_0=\omega_{LH}+\omega_{IC}$, $\mathbf{k}=\mathbf{k}_{LH}+\mathbf{k}_{IC}$ for propagation $\cos^2\theta\,(m_i/m_e)\lesssim 1$ the ion-cyclotron wave has to propagate backwards, $k_\perp^2\rho_i^2>1$. Maximization of the growth rate (107) gives $k_\perp^2\rho_i^2\sim 1.5$. Consequently, relevant parameters for EBT-S calculations are ($k_\perp\equiv k_d$): $k_d r_{De}\sim 0.2$, $k_d\rho_e\sim 0.1$, and $k_d r_{Di}\sim 0.04$. For typical parameters of EBT-S in region III, $n_e=10^{12}\,\mathrm{cm}^{-3}$, $B=0.5\times 10^4\,T$, and $T_i\sim 25$ eV, for the perpendicular wavelength of the primary excited LHW we obtain around 1 cm. Knowing $k_\perp$ we can easily find k_z from (20) for a given $\omega_0-\omega_{LH}^*(r)$, or for a given k_z we can find a distance Δr from the surface at r at which the k_z mode is excited. We note that here $\omega_0-\omega_{LH}^*(r)\gg\omega_{IC}(r)$ so that excitation takes place relatively far from strict resonance $\omega_0=\omega_{LH}(r)$, which corresponds to excitation of well-defined ion-cyclotron waves. Excitation of an ion-cyclotron quasimode that takes place in the region where $\omega_0-\omega_{LH}^*(r)\ll\omega_{IC}(r)$ is not of interest here because it has a higher threshold.[20]

In (107) γ_{LH} is the linear damping rate of a LHW, including collisional and perpendicular ion-Landau dissipation (zone III, Fig. 5):

$$\gamma_{LH}=\nu_{ei}\left(\frac{\omega_{pe}}{\Omega_e}\right)^2\left(1+\frac{\omega_{pe}^2}{\Omega_e^2}\right)^{-1} +\left(\frac{\pi}{8}\right)^{1/2}\frac{\omega_{pi}}{(kr_{De})^3}\left(\frac{T_e}{T_i}\right)^{3/2}\left(1+\frac{\omega_{pe}^2}{\Omega_e^2}\right)^{-2} \times\exp\left(-\frac{T_e^2}{T_i^2}\frac{1}{2k^2 r_{De}^2}\right). \quad (108)$$

In regions I and II (see Fig. 5), the dominant noncollisional dissipation is parallel electron Landau damping.[11] The collisional wavenumber, obtained from (108) equating collisional and perpendicular ion-Landau damping, is

$$k_{coll}r_{De}\sim\frac{1}{\sqrt{\pi}}\left(\frac{T_e}{T_i}\right)^{1/2}\left[\ln\sqrt{\pi}\left(\frac{\omega_{LH}}{\nu_{ei}}\right)\left(\frac{\Omega_e}{\omega_{pe}}\right)^2\right]^{-1/2}, \quad (109)$$

which for EBT-S in zone III (Fig. 6) gives $k_{coll}r_{De}\sim 0.8$. Consequently, primary decay will be in a strong collisional region ($k_d<k_{coll}$) that significantly minimizes the dissipative threshold. This dissipative threshold,[44] however, cannot be representative because even a minimized convective threshold gives higher values as will be shown in what follows.

Taking into account that $k^2 r_{De}^2\ll 1, (1+\mathrm{Re}\,\chi_e)^2\sim(kr_{De})^{-4}$, so that the threshold for excitation of a LHW coupled to a backward ion-cyclotron wave ($k_\perp^2\rho_i^2>1$) has the form

$$\frac{E_{0x,T}^2}{4\pi n_e T_e} = 8\frac{V_{LH}V_{IC}^{(n)}}{L_z^2}\frac{1}{\omega_{LH}\Omega_i}\frac{T_i}{T_e} \times\left(\frac{\omega_0}{\omega_{pe}}\right)^2\left(\frac{\Omega_e}{\omega_{pe}}\right)^2\frac{1}{nA_n(k_\perp^2\rho_i^2)}. \quad (110)$$

Here V_{LH} is the group velocity of the lower-hybrid wave along the z axis:

$$\mathbf{V}_{LH} = \omega_{LH}\left(\frac{k_z}{k^2}\right)\frac{m_i}{m_e}\left\{0, -\frac{k_y k_z}{k^2}, 1\right\}. \quad (111)$$

If instead of a backward ion-cyclotron wave an ion-Bernstein wave is excited, we have

$$\frac{E_{0x,T}^2}{4\pi n_e T_e} = 8\frac{V_{LH}V_{IB}^{(n)}}{L^2}\frac{1}{\omega_{LH}\Omega_i}\frac{T_i}{T_e}\frac{(n\Omega_i)^4}{(k_y r_{De})^4(\omega_{pe}\cos\theta)^4} \times\left(\frac{\omega_0}{\omega_{pe}}\right)^2\left(\frac{\Omega_e}{\omega_{pe}}\right)^2\frac{1}{nA_n(k_\perp^2\rho_i^2)}; \qquad \cos^2\theta\frac{m_i}{m_e} \ll 1. \quad (112)$$

The ratio between thresholds (112) and (110) is $(k_y r_{De}/n)^4(\omega_{pi}/\Omega_i)^4(m_i/m_e)^2\cos^4\theta$. For propagation defined by $\cos^2\theta(m_i/m_e)\sim 10^{-1}$, and for typical parameters of EBT-S, we see that an ion-cyclotron wave ($n=1$) has a threshold nearly four times lower than IBM.[1] If $n=2$, thresholds are approximately equal, and for $n>3$, the decays LHW + IBM$^{(n)}$ have lower thresholds. Note, however, that as n increases, the thresholds, in principle, also increase [see (110) and (112)].

Finally, in the left-hand side region near point 4 (see Fig. 6), it is possible to excite two lower-hybrid waves. The parametric growth rate has the form

$$(\gamma+\gamma_{LH}) = \tfrac{1}{2}\omega_{LH}\left(\frac{ek_y E_{0x}}{m_e\omega_0\Omega_e}\right)\left(\frac{k_{0x}}{k_y}\right)^2. \quad (113)$$

In (113) the coupling mechanism is the $\mathbf{E}_0\times\mathbf{B}_0$ radio-frequency electron drift. For the corresponding threshold value for convection of LHW along the z axis [see (111)] we have

$$\frac{E_{0x,T}^2}{4\pi n_e T_e} = \frac{2}{(k_y r_{De})^4}\left(\frac{\omega_0}{\omega_{pe}}\right)^2\left(\frac{\Omega_e}{\omega_{pe}}\right)^2\left(\frac{k_y}{k_{0x}}\right)^4\left(\frac{k_z}{k_y}\right)^2\left(\frac{m_i}{m_e}\right)^2\left(\frac{r_{De}}{L_z}\right)^2. \quad (114)$$

Let us now apply the expressions obtained to calculate the thresholds, using EBT-S parameters in the appropriate zones (Fig. 6). In zone I we still assume $n_e\sim 10^{10}$ cm^{-3}, $B_0 = 0.1$ T, and $T_e\sim 25$ eV. In the case of excitation of a G–T mode coupled to an ion-cyclotron wave (100), the cutoff density for propagation $\cos^2\theta(m_i/m_e)\gtrsim 10$ is $n_e\lesssim 4\times 10^{11}$ cm^{-3} and for $\cos^2\theta(m_i/m_e)\gtrsim 10^3$, $n_e\lesssim 4\times 10^9$ cm^{-3}. Consequently, we shall primarily be interested in G–T modes propagating at larger angles $\cos\theta\gtrsim 0.05$. For the above parameters and for $L\sim 1$ cm from (100) for the case of excitation of a G–T mode coupled to a backward ion-cyclotron wave, we have $E_{0z,T}\sim 1$ kV/cm, and in the case of excitation of an IB mode, $E_{0z,T}\sim 50$ V/cm for $n=1$. We note that for higher harmonics the threshold increases as $(n^{3/2})/A_n^{1/2}$ in the case of IB modes and as $(1/nA_n)^{1/2}$ in the case of backward ion-cyclotron waves. In the case of dominant $\mathbf{E}_0\times\mathbf{B}_0$ coupling (between points 1 and 3 in Fig. 6) from (102), we have $E_{0x,T}\sim 250$ V/cm for excitation of backward ion-cyclotron waves and $E_{0x,T}\sim 20$ V/cm for excitation of IB modes if $n=1$. In this zone we assumed $n_e\sim 10^{11}$ cm^{-3}, $B_0\sim 0.3$ T, and $T_e\sim 100$ eV.

In the region left of point 2 (Fig. 6), it is possible to excite two G–T modes. If the dominant coupling is E_{0z}, from (105) the threshold is $E_{0z,T}\sim 1500$ V/cm, with $n_e\sim 10^{10}$ cm^{-3}, $T_e\sim 100$ eV, and $L\sim 10$ cm. Here $\mathbf{E}_0\times\mathbf{B}_0$ coupling in this region is stronger and gives somewhat lower thresholds, around 500 V/cm [see (106)].

Finally, let us investigate threshold values for excitations in zone III in which we shall assume $n_e\sim 10^{12}$ cm^{-3}, $T_e\sim 500$ eV, and $B_0\sim 0.7$ T. In the case of excitation of LHW coupled to backward propagating ion-cyclotron waves, (110) gives $E_{0x,T}\gtrsim 300$ V/cm. If an ion-Bernstein mode is excited, the threshold is around 100 V/cm; in the case of simultaneous excitation of two LHW, it is around 600 V/cm [see (114)].

Once it is excited in a particular zone, a G–T mode or LHW can further decay through two different secondary channels. The first secondary channel is decay of a primary excited G–T (LHW) mode into another G–T (LHW) coupled to a low-frequency mode; the second one is the decay of the G–T (LHW) modes into two other G–T (LHW) modes. As seen from (46), the driver pump depletion length depends on the energy content in a first cascade W_1. If primary decay (G–T + IC) is of the same nature as secondary decay (G–T^1 + IC^1), then $W(0)\gtrsim W_1$ (see Ref. 10). Consequently, for the driver pump depletion length we have $L = V_{0i}/2\,\mathrm{Im}\,k_0 V_H$ or, in the case of absolute[25] instabilities, $L = V_{0i}/2\gamma$. If secondary decay is of a different nature (G–T^1 + G–T^2), then, if its growth rate for a given intensity of the electric field is larger than the growth rate of primary decay, W_1 could be significantly smaller compared to $W(0)$, thus leading to larger L and consequently to less efficient nonlinear absorption. Comparison of primary and secondary growth rates in k space is out of the scope of the present paper. Instead, we give estimates of depletion length under the assumption that secondary and primary decays are of the same nature. Thus, we give a minimum possible value for L.

In the case of excitation of a G–T mode coupled to an ion-Bernstein mode in zone I (Fig. 6), the nonlinearly absorbed power density is [see (53)]

$$Q^{conv} = \frac{\mu_{L1}^2 L^3}{4V_{IB}^2 V_{G-T}}(kr_{De})^4\left(\omega_{pe}\Omega_i\cos\theta\frac{T_e}{T_i}nA_n(k_\perp^2\rho_i^2)\right)^2 W_{0,THR}. \quad (115)$$

Here, in the coupling coefficient μ_{L1}^2 (95) $[1+\mathrm{Re}\,\chi_e(\omega,\mathbf{k})]\sim-(\omega_{pi}/n\Omega_i)^2\cos^2\theta$, $\cos^2\theta\lesssim(m_e/m_i)$. If the $\mathbf{E}_0\times\mathbf{B}_0$ coupling mechanism is dominant, the absorbed power density could be obtained from (115) by the substitution $\mu_{L1}\rightarrow\mu_{L2}$ [(96)]. Knowing the nonlinearly absorbed power density, it is easy to find the driver pump depletion length [compare to (46)]:

$$L^{\mathrm{conv}}=V_{0,i}\,[W_0(0)/Q^{\mathrm{conv}}]. \tag{116}$$

In (116), $V_{0,i}$ is the x component of the group velocity of a slow mode[41,45] in LHFR ($\Omega_i<\omega_0<\omega_{pe}<\Omega_e$), given by (see Fig. 5)

$$\mathbf{V}_{SW}=\left\{\frac{c}{n_\parallel}\frac{\omega_0}{\omega_{pe}},0,\frac{c}{n_\parallel}\right\}, \tag{117}$$

where $n_\parallel=ck_\parallel/\omega_0$ is the parallel index of refraction that must satisfy the accessibility[41,45] criterion

$$n_\parallel^2>1+\omega_{pe}^2/\Omega_e^2. \tag{118}$$

The nonlinear absorbed power density in zone II, caused by the excitation of two G–T modes, is

$$Q^{\mathrm{conv}}=(L^3/16V_{\mathrm{G\text{-}T}}^3)(\mu_{H2}\omega_{pe}\cos\theta)^4W_{0,\mathrm{THR}}. \tag{119}$$

In zone I the threshold for this decay is significantly higher (see Table I) and Q^{conv} is smaller. It could be obtained from (119) by substitution $\mu_{H2}\rightarrow\mu_{H1}$.

In zone III (Fig. 6) excitation of LHW takes place with thresholds in the domain of available intensities of electric field (note that $E_{0z}/E_{0x}\sim\omega_0/\omega_{pe}$ gives significant enhancement of component E_{0x} in zone III, which actually is a driver pump). The nonlinearly absorbed power density for the case when both modes are well defined ($\omega_{\mathrm{LH}}\gg\gamma_{\mathrm{LH}}$, $\omega_{\mathrm{IC}}\gg\gamma_{\mathrm{IC}}$) is given by

$$Q^{\mathrm{conv}}=\frac{L^3}{V_{\mathrm{IC}}^2V_{\mathrm{LH}}}\left(\frac{E_{0x}^2}{4\pi n_eT_e}\right)^2(kk_yr_{De}^2)^4\left(\omega_{\mathrm{LH}}\Omega_i\frac{T_e}{T_i}\right)^2\left(\mathrm{Re}\,\chi_e(\omega,\mathbf{k})\frac{\omega_{pe}^2}{\omega_0\Omega_e}\right)^4\frac{nA_n(k_\perp^2\rho_i^2)}{64}W_{0,\mathrm{THR}}. \tag{120}$$

In (120), $\mathrm{Re}\,\chi_e(\omega,\mathbf{k})\sim(kr_{De})^{-2}$ if an ion-cyclotron wave is excited or $\mathrm{Re}\,\chi_e(\omega,\mathbf{k})\sim-(\omega_{pi}/n\Omega_i)^2\cos^2\theta$, $\cos^2\theta\lesssim(m_e/m_i)$, if an ion-Bernstein mode is excited.

Finally, for the case of excitation of two LHW, the absorbed energy has the form

$$Q^{\mathrm{conv}}=\frac{L^3}{16V_{\mathrm{LH}}^3}\left(\omega_{\mathrm{LH}}\frac{ek_yE_{0x}}{m_e\omega_0\Omega_e}\right)^4\left(\frac{k_{0x}}{k_y}\right)^8W_{0,\mathrm{THR}};\qquad k_y>k_{0x}. \tag{121}$$

Let us now give estimates for the driver pump depletion lengths in different zones (Figs. 5 and 6) in the upper limit of applicability of a weak turbulence theory $\gamma\lesssim\Omega_i$, for the case of absolute instability or $\mathrm{Im}\,k_0V_H\lesssim\Omega_i$ (H denotes G–T mode or LHW) in the case of convective instabilities. Under such a condition, the depletion length takes the simple form

$$L=\frac{c}{2n_\parallel\Omega_i}\frac{\omega_0}{\omega_{pe}}. \tag{122}$$

For the parallel index of refraction of a slow wave at the boundary layer of EBT we shall assume $n_{\parallel0}\sim4$. This gives $\lambda_{0z}\sim30$ cm and $\lambda_{0\perp}\sim10$ cm. Taking typical parameters of EBT-S in zones I, II and III from (122) we have $L_{\mathrm{I}}\sim100$ cm $\sim10\lambda_{0\perp}$, $L_{\mathrm{II}}\sim\lambda_{0\perp}$, and $L_{\mathrm{III}}\lesssim0.5\lambda_{0\perp}$. Accordingly, we can conclude that in zone I the driver pump power absorption is negligible while in zone II, where coupling is dominated by $\mathbf{E}_0\times\mathbf{B}_0$, absorption caused by the decay $\omega_{\mathrm{G\text{-}T}}+\omega_{\mathrm{IB}}$ (see Table I) can be significant. We expect strong nonlinear absorption in zone III through excitation of LHW coupled to ion-Bernstein modes (see Table I). This can significantly influence linear conversion[11] in which all the driver pump power is supposed to reach the throat of the mirror section where linear mode conversion takes place (Fig. 5). It is to be noted, however, that the above estimates are lower limits. Taking into account secondary decay of different types, the influence of plasma inhomogeneity on buildup of turbulence, low-frequency fluctuations induced by other sources,[46] etc., will give larger L and, consequently, decrease nonlinear absorption.

TABLE I. Thresholds for parametric decay $\omega_0=\omega_1+\omega_2$ for various driver pump frequencies and decay products for EBT-S parameters and driver pump depletion length.

ω_0	ω_1	ω_2	E_T, zone I	E_T, zone II	E_T, zone III
$\omega_{\mathrm{G\text{-}T}}$	$\omega_{\mathrm{G\text{-}T}}$	ω_{IC}	1 kV/cm		
$\omega_{\mathrm{G\text{-}T}}$	$\omega_{\mathrm{G\text{-}T}}$	ω_{IB}	50 V/cm		
$\omega_{\mathrm{G\text{-}T}}$	$\omega_{\mathrm{G\text{-}T}}$	ω_{IC}		250 V/cm	
$\omega_{\mathrm{G\text{-}T}}$	$\omega_{\mathrm{G\text{-}T}}$	ω_{IB}		20 V/cm	
$2\omega_{\mathrm{G\text{-}T}}$	$\omega_{\mathrm{G\text{-}T}}$	$\omega_{\mathrm{G\text{-}T}}$	1500 V/cm		
$2\omega_{\mathrm{G\text{-}T}}$	$\omega_{\mathrm{G\text{-}T}}$	$\omega_{\mathrm{G\text{-}T}}$		500 V/cm	
ω_{LH}	ω_{LH}	ω_{IC}			300 V/cm
ω_{LH}	ω_{LH}	ω_{IB}			100 V/cm
$2\omega_{\mathrm{LH}}$	ω_{LH}	ω_{LH}			600 V/cm
Driver pump depletion length			100 cm	10 cm	$\lesssim5$ cm

VI. ION-CYCLOTRON HARMONIC RESONANCES

The application of radio-frequency waves in the ion-cyclotron frequency range (ICFR) has attracted considerable attention in thermonuclear fusion research. This concept has been intensively studied in tokamaks (see, for example, Refs. 47 and 48) and in EBT (see, for example, Refs. 49 and 50). In this frequency range we have two mode conversion

heating regimes: minority ion (H, ^{3}He) heating at the fundamental ion-cyclotron frequency and majority ion (deuterons) heating at the second or higher ion-cyclotron harmonic layer. In linear conversion, a fast magnetosonic wave is converted into an ion-Bernstein mode at $\omega = n\Omega_i$,[51] $n = 2, 3\ldots$, or at $\omega = \Omega_{i1} + \Omega_{i2}$ in a two ion-species plasma[52] (Ω_{i1}, Ω_{i2}, ion-cyclotron frequency of majority and minority ions, respectively). In nonlinear mode conversion, treated in this paper, a fast magnetosonic wave decays into longitudinal ion-cyclotron harmonic waves mutually coupled and/or a harmonic wave coupled to a low-frequency ion-acoustic quasimode.

We study excitation of plasma modes with frequencies near the local ion-cyclotron harmonic frequency assuming that the driver pump frequency is $\omega_0 = m\Omega_i + n\Omega_i = S\Omega_i$ ($m, n = 1, 2, \ldots$). The geometry of interaction (see Fig. 7) is defined by the driver pump electric field $\mathbf{E}_0 = \{0, E_{0y}, 0\}$ in the vacuum and the magnetic field vector $\mathbf{B}_0 = \{0, 0, B_0\}$. In the linear resonance layers, because of the inhomogeneity along the x axis, the driver pump electric field will have an E_{0x} component caused by WKB processes. Consequently, $E_0 = \{E_{0x}, E_{0y}, 0\}$, $E_{0x} \gg E_{0y}$. This component, E_{0x}, is actually the electric field of a linearly converted ion-Bernstein mode in the corresponding resonance layer (Figs. 7 and 8). For the wave vector of the excited ion-cyclotron harmonic wave we shall assume $\mathbf{k} = \{k_x, 0, k_z\}$, $k_z/k_x \ll 1$ [in ICFR, perpendicular $E_{0\perp}$ radio-frequency ion drift is the basic coupling mechanism (7)]. For this geometry, the coupling coefficient [see (7) and (8)] is

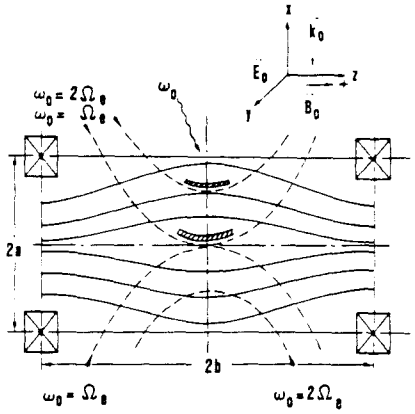

FIG. 7. Geometry of EM wave–EBT plasma interaction in ICFR. The angular frequency of the driver pump (fast magnetosonic wave) is chosen to be equal to the ion-cyclotron frequency at the axis of EBT. For $\omega_0 \gg \Omega_e(0)$, interaction takes place at higher ion-cyclotron harmonics resonance layers. Shaded areas denote regions of nonlinear interaction located somewhat further from linear conversion surfaces, $\omega_0 = \Omega_e(0)$, $\omega_0 = 2\Omega_e(r)$.

$$\mu_H^2 = \frac{e_i^2 k_x^2 E_{0x}^2}{m_i^2[\phi(S)]^2} \frac{[k_{0x}(2k_x - k_{0x}) + k_{0z}(2k_z - k_{0z})]^2}{(k_x^2 + k_z^2)\,[(k_x - k_{0x})^2 + (k_z - k_{0z})^2]}, \tag{123}$$

where [$\omega_0 \sim S\Omega_i$, see (A17)]

$$\phi(S) = \omega_0^2 - \Omega_i^2 = (S+1)\,\Omega_i \left((S-1)\Omega_i + S\Omega_i \frac{T_e}{T_i} \frac{A_s(k_\perp^2 \rho_i^2)}{1 + k^2 r_{De}^2 - A_0(k_\perp^2 \rho_e^2) + (T_e/T_i)[1 - A_0(k_\perp^2 \rho_i^2)]} \right). \tag{124}$$

The parametric growth rate for the excitation $\omega_0 = l\Omega_i + m\Omega_i$ ($l, m = 1, 2, \ldots$) by a fast magnetosonic wave (see Fig. 8) is given by

$$(\gamma + \gamma_{IC}^{(l)})(\gamma + \gamma_{IC}^{(m)}) = \mu_H^2 \frac{(kr_{De})^4}{16\Omega_i^6} \left(\frac{T_i}{T_e}\right)^2 \times \left(\sum_{l=1}^{\infty} \sum_{m=1}^{\infty} \frac{(lm)^3 A_l(k_\perp^2 \rho_i^2) A_m(k_\perp^2 \rho_i^2)}{(\omega^2 - m^2\Omega_i^2)^2 (\omega^2 - l^2\Omega_i^2)^2} \right)^{-1}. \tag{125}$$

In (125), ω takes the form (A18) for the case of excitation of ion-cyclotron harmonics and (A17) in the case of IB mode harmonics. For the EBT environment, (125) will be analyzed for $l = m = 1$, i.e., when $\omega_0 = 2\Omega_i$. In this case, excitation of two ion-cyclotron waves (IBM) propagating in nearly opposite directions ($\mathbf{k}_0$) is possible. Then (125) reduces to [compare to (60)]

$$(\gamma + \gamma_{IC}^{(l)})/\Omega_i = \mu_H (kr_{De})^2 (T_e/T_i) A_1(k_\perp^2 \rho_i^2). \tag{126}$$

The maximum growth is obtained for $k\rho_i \sim 1.2 (A_1 \sim 0.22)$.

For the convective threshold caused by the plasma inhomogeneity we have

$$\frac{E_{0x,T}^2}{4\pi n_e T_e} = \frac{3}{2} \left(\frac{\Omega_i}{\omega_{pi}}\right)^2 \frac{1}{(kr_{De})^3} \left(\frac{T_i}{T_e}\right)^2 \frac{1}{A_1(k_\perp^2 \rho_i^2)} \frac{V_{IC,x}^{(l)}}{L_x \Omega_i}. \tag{127}$$

In the nth ion-cyclotron harmonic layer it is possible to excite the nth harmonic coupled to some low-frequency mode. In resonant excitation, the only possible low-frequency mode is a low-frequency ion-acoustic wave. The corresponding coupling coefficient is

$$\mu_L^2 = \frac{e_i^2 k_x^2 E_{0x}^2}{4m_i^2[\phi(n)]^2} [1 + \mathrm{Re}\,\chi_e(\omega, \mathbf{k})]^2, \tag{128}$$

with

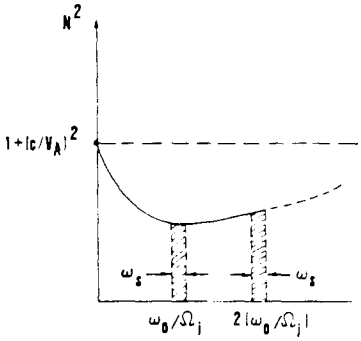

FIG. 8. The index of refraction, $N = ck_0/\omega_0$, of the fast magnetosonic wave for nearly perpendicular incidence $\cos^2\theta_0 (m_i/m_e) \lesssim 1$. The low-frequency ion-acoustic wave is indicated by ω_s. Here c and V_A are the speed of light in vacuum and the Alfvén speed, respectively. Shaded areas correspond to shaded areas in Fig. 6.

$$1 + \mathrm{Re}\,\chi_e(\omega, \mathbf{k}) = 1 + \frac{1}{k^2 r_{De}^2} - \frac{\omega_{pi}^2 \cos^2\theta}{\omega^2},$$

$$\cos^2\theta \frac{m_i}{m_e} \lesssim 1. \tag{129}$$

Note that for $\cos^2\theta(m_i/m_e) \lesssim 1$ the low-frequency ion-acoustic wave is heavily damped (resonant quasimode $\gamma_s \sim \omega_s$). For the growth rate we obtain

$$(\gamma + \gamma_{IC}^{(n)})(\gamma + \gamma_s) = (\mu_L^2/8)(kr_{De})^4 \omega_s\,(T_i/T_e) \times \left(\sum_{n=1}^{\infty} \frac{(n\Omega_i)^3 A_n(k_\perp^2 \rho_i^2)}{(\omega^2 - n^2\Omega_i^2)^2} \right)^{-1}, \tag{130}$$

where $\omega_s = kV_s \cos\theta$ and $V_s = (T_i/m_e)^{1/2}$. In this case, as seen from (130), $\gamma \propto E_{0x}^2$ in contrast to $\gamma \propto E_{0x}$, which is valid for the case of excitation of well-defined modes.

In the principal ion-cyclotron harmonic layer from (130) we have

$$\frac{\gamma + \gamma_{IC}^{(1)}}{\Omega_i} = \frac{\mu_L^2}{2} (kr_{De})^4 \frac{T_e}{T_i} A_1(k_\perp^2 \rho_i^2), \tag{131}$$

and for the threshold

$$\frac{E_{0x,T}^2}{4\pi n_e T_e} = 8 \left(\frac{\Omega_i}{\omega_{pi}}\right)^4 \frac{1}{(kr_{De})^2} A_1(k_\perp^2 \rho_i^2) \frac{T_i}{T_e} \frac{V_{IC}^{(1)}}{L\Omega_i}. \tag{132}$$

From (127) taking $n_e \sim 10^{11}$ cm^{-3}, $T_e \sim 500$ eV, and $L \sim 1$ cm, we have $E_{0x} \gtrsim 50$ V/cm, and from (132) which is valid for the regions near the EBT axis, $n_e \sim 10^{12}$ cm^{-3}, $E_{0x} \gtrsim 250$ V/cm.

For the nonlinearly absorbed power density in the $\omega_0 = 2\Omega_i$ resonance layer, we have

$$Q^{\mathrm{conv}} = \frac{L^3}{V_{IC}^{(1)3}} (kr_{De})^8 \left(\mu_H \Omega_i \frac{T_e}{T_i} A_1(k_\perp^2 \rho_i^2) \right)^4 W_{0,\mathrm{THR}}, \tag{133}$$

and in the $\omega_0 = \Omega_i$ resonance layer

$$Q^{\mathrm{conv}} = \frac{L}{V_{IC}^{(1)}} \frac{\mu_L^4}{4} (kr_{De})^8 \left(\Omega_i \frac{T_e}{T_i} A_1(k_\perp^2 \rho_i^2) \right)^2 W_{0,\mathrm{THR}}. \tag{134}$$

The driver pump depletion length in ICFR has the form

$$L^{\mathrm{conv}} = V_x [W_0(0)/Q^{\mathrm{conv}}]^{-1}, \tag{135}$$

where V_x is the x component of the group velocity of a fast magnetosonic wave given by

$$\mathbf{V}_{FM} = \left\{ V_A \frac{k_x}{k}, 0, V_A \frac{k_z}{k} \right\}, \quad V_A = \frac{B_0}{\sqrt{4\pi n_i m_i}}, \tag{136}$$

with V_A being the Alfvén speed. For the typical parameters on the axis of EBT and for $f_0 \gtrsim 30$ MHz ($\lambda_0 \lesssim 10$ m) from (135), in the upper limit of applicability of weak turbulence theory $\gamma \lesssim \omega_s \sim 10^{-1}\Omega_i$, we have $L^{\mathrm{conv}} \gtrsim 100$ cm, comparable to the vacuum wavelength of the driver pump. Consequently, we can conclude that nonlinear absorption can play a significant role in ICFR.

VII. DISCUSSION AND CONCLUSION

In this review we presented a nonlinear mode conversion theory for plasma parameters and geometry of the interaction typical for the EBT environment. Pump wave thresholds were calculated for decay into a variety of plasma waves. The results are shown in Tables I and II. The condition for validity of the presented theory (weak parametric turbulence, $\gamma_0, \gamma_n \ll \omega_L \sim \omega_{LH}$) in the ECFR is

$$E_{EB} \ll \left(\frac{\omega_{pe}}{\Omega_e}\right) \left(\frac{\omega_{LH}}{\gamma_{EB}}\right) \left(\frac{\omega_{LH}}{\gamma_{LH}}\right)^{1/2} E_0, \quad \gamma > \gamma_{EB}, \gamma_{LH}, \tag{137}$$

for the case of excitation of well-defined modes, and

$$E_{EB} \ll \left(\frac{\omega_{LH}}{\gamma_{EB}}\right) \left(\frac{\omega_{pe}}{\Omega_e}\right) E_0, \quad \gamma_{EB} < \gamma \lesssim \gamma_{LH}, \tag{138}$$

for the excitations of quasimodes. Also, validity of the theory is based on the assumption of weak electric fields of the low-frequency mode so that the low-frequency waves will not influence the power balance equation written for high-frequency waves. Utilizing the Manley–Rowe relation, it is easy to show that

$$E_{LH}^2 \sim \frac{\omega_{LH}^3 \Omega_e}{\omega_{pi}^2 \omega_{pe}^2} \left(\frac{\gamma_{EB}}{\gamma_{LH}}\right) E_{EB}^2. \tag{139}$$

Typical values for EBT-S and obtained values for E_{EB} give for E_{LH} approximately 10 V/cm. This is, however, the upper limit because in (139) it was assumed that all energy in N low-frequency cascades is concentrated in a single one. Accordingly, it is not likely that such a field can produce low-frequency turbulence.

At present, EBT operates in two modes in ECFR. When operated up to 60 kW at 18 GHz with the magnetic field in the central midplane of 0.5 T, it is called EBT-1. If operated with 200 kW at 28 GHz with $B_0 \sim 0.7$ T, it is called EBT-S. Further, 24 mirror sections are fed by a single gyrotron. In EBT-1, consequently, only 2 kW are available per section, which is not sufficient to produce any of the considered parametric processes. In EBT-S, the available power flux in the second electron-cyclotron layer is approximately 20 W/cm^2 ($E_0 \lesssim 120$ V/cm) and in the principal electron-cyclotron layer approximately 4 W/cm^2 ($E_0 \lesssim 60$ V/cm). These values for the electric field are not enough to produce parametric processes in the long-wavelength region ($k^2\rho_e^2 \ll 1$). However, in the narrowband short-wave length region, we expect that

TABLE II. Thresholds and saturation electric field of a high-frequency mode for parametric decay $\omega_0 = \omega_1 + \omega_2$ for various pump frequencies and decay products for EBT-S parameters.

ω_0	ω_1	ω_2	$k\rho_e$	E^r	$E_{\omega 1}$
$2\Omega_e$	Ω_{EB}	Ω_{EB}	0.1	350 V/cm	1.5 kV/cm
$2\Omega_e$	Ω_{EB}	Ω_{EB}	1.0	50 V/cm	200 V/cm
$2\Omega_e$	$2\Omega_{EB}$	Ω_{LH}	0.1	600 V/cm	3 kV/cm
$2\Omega_e$	$2\Omega_{EB}$	Ω_{LH}	1.0	60 V/cm	300 V/cm
Ω_e	Ω_{EB}	Ω_{LH}	1.0	40 V/cm	200 V/cm
Ω_e	Ω_{EB}	Ω_{LH}	0.1	400 V/cm	2 kV/cm
ω_{UH}	ω_{UH}	ω_{LH}	0.1	70 V/cm	2 kV/cm

instabilities evolve to a significant turbulence level. For future experiments with $P_0 \sim 600$ kW, this will also be true for the long-wavelength region.

In the present experiments, in the second harmonic EC layer, we expect observation of the second and principal harmonic EBM in a narrow wavelength region $\lambda_{EB} \sim 1$ mm (short-wavelength region with respect to pump $\lambda_0 \sim 1$–2 cm). Also we expect the observation of a number of ion-cyclotron harmonics in both principal and second harmonic EC layers with wavelengths $\lambda_{IB} \sim 1$ cm.

When comparing parametric absorption with linear damping, it is important to take account of the spatial location (away from resonance) where parametric absorption can take place, since the wave amplitude is very small exactly at the resonance layer (because of the linear absorption). The spatial extent of the parametric absorption layer can be estimated from $\omega_0 - \Omega_e(x) \lesssim \omega_{LH}$ (or kV_{Ti} for ion-acoustic wave excitation). Expanding $\Omega_e = \Omega_e(0)\ (1 + \Delta x/L_B)$ gives $\Delta x \lesssim L_B\ (\omega_{LH}/\Omega_e) \approx 1/40\ L_B$, a distance of a centimeter in EBT.

Although in this paper the standard heating scheme was considered (Fig. 1), the obtained results are also valid for fundamental and "scratch" heating schemes.[53]

In a future reactor-size EBT, an electric field of 1 kV/cm per section will be available so that inequalities (137) and (138) cannot be satisfied. Accordingly, parametric processes must be calculated in a strong coupling regime when the present theory is generalized to include coupling between cascades.

Finally, the existence of parametric processes will not only affect absorption characteristics of the system, but will also change the spectrum of waves in the system leading, for example, to direct heating of ions, as well as preferential heating of different parts of the electron distribution function. These processes are all under investigation.

In LHFR, the feasibility of heating EBT plasma by linear conversion processes at the throat of the mirror section was examined recently in Ref. 11. In this review we have assumed that the parallel index of refraction of the plasma at the frequency of the drive pump, slow lower-hybrid mode, satisfies $n_{0\|\max} > n_{0\|} > \max(n_{0\|ac}, n_{0\|L})$. Here $n_{0\|ac}$ is given by the right-hand side of (118). By requiring $n_{0\|} > n_{0\|L}$ ($n_{0\|L}$ defines the parallel index of refraction when electron Landau damping of LHW in zones I and II is negligible), we exclude competition between parametric absorption and electron-Landau[54] absorption in zones I and II. Further, $n_{0\|\max}$ is determined by the condition that linear conversion take place at least 2–3 cm from the EBT axis.[11] Processes inside this distance (zone IV, Fig. 5) are not considered in this study.

In the ion-cyclotron frequency range we have considered processes that take place at $\omega_0 = 2\Omega_i$ and $\omega_0 = \Omega_i$ (at the axis of EBT).

As a characteristic of nonlinear absorption, we utilized the concept of the driver pump depletion length. It was shown that in both LHFR and ICFR the depletion length can be equal to or less than the vacuum wavelength of the driver pump, demonstrating the effectiveness of parametric absorption in these frequency ranges.

Direct heating of ions through parametrically excited ion-Bernstein modes can directly influence linear conversion processes in LHFR by removing the linear conversion layer further from the EBT axis, thus preventing the linear heating of the core. In ICFR, development of nonlinear processes that takes place in front of the linear conversion surface (see Fig. 7) can lead to enhanced bulk plasma heating through cascading processes.

Finally, let us say that although parametric processes at the EBT boundary layer do not play any significant role from the aspect of overall driver pump power deposition, they can influence the apparent spectrum of a driver pump by changing the propagation characteristics. From the other side, parametrically excited ion-Bernstein modes can enhance the initial level of low-frequency fluctuations (for example, fluctuations caused by the drift-instabilities)[46] which, in turn, can lead to additional scattering of the driver pump.

ACKNOWLEDGMENTS

This work was supported by the U. S. Department of Energy.

APPENDIX: LONGITUDINAL CYCLOTRON WAVES

In order to evaluate dielectric permittivities of electron-cyclotron waves entering in (1), we will utilize the Ginzburg–Rukhadze[55] dispersion relation for Maxwellian longitudinal plasma modes in the following form (with some changes in notation, it is identical to the Fried–Conte dispersion relation[56])

$$\epsilon(\omega, \mathbf{k}) = \mathrm{Re}\,\epsilon + i\,\mathrm{Im}\,\epsilon = 1 + \sum_{\alpha} \frac{1}{k^2 r_{D\alpha}^2} \times \left[1 - \sum_{l=-\infty}^{+\infty} \frac{\omega}{\omega - l\Omega_\alpha} A_l(k_\perp^2 \rho_\alpha^2) \times \Gamma_+\left(\frac{\omega - l\Omega_\alpha}{|k_z| V_{T\alpha}} \right) \right] + i\epsilon_{\mathrm{coll}}, \tag{A1}$$

where

$$\Gamma_+(x) = x \exp\left(-\frac{x^2}{2}\right) \int_0^x \exp\left(\frac{y^2}{2}\right) dy - i\sqrt{\pi/2}\, x \exp(-x^2/2),$$

and $A_l(x) = I_l(x) \exp(-x)$. Here $I_l(x)$ is the modified Bessel function of the first kind of order n, and $r_{D\alpha}$ and ρ_α are the Debye and Larmor radii of α particles, respectively. The wavenumbers normal and parallel to the magnetic field vector B_0 are denoted by k and k_z, respectively.

In the EC harmonics frequency range, $\omega \sim n|\Omega_e|$, in (A1), the response of the electron plasma component is dominant, so that for perpendicular propagation ($k_z \to 0$, electron-Bernstein mode), taking into account that $\Gamma_+(x) \to 1$, $x \to \infty$, we have

$$\epsilon(\omega, \mathbf{k}) = 1 + \frac{1}{k^2 r_{De}^2} \left(1 - \sum_{l=-\infty}^{+\infty} \frac{\omega}{\omega - l\Omega_e} \times A_l(k^2 \rho_e^2) \right) + i\epsilon_{\mathrm{coll}}. \tag{A2}$$

In EBT-S plasma, we have typically $\Omega_e \sim 1.6\omega_{pe}$ so that $\rho_e < r_{De}$. Taking this into account along with $A_0(x) \to 1$ for $x \ll 1$, and $A_0(x) \to 0$ for $x \gg 1$ from (A2), we easily obtain a result[18] that is valid for arbitrary wavelengths:

$$\mathrm{Re}\,\epsilon(\omega, \mathbf{k}) = 1 - 2\sum_{l=1}^{\infty} \frac{l^2 A_l(k^2\rho_e^2)\omega_{pe}^2\Omega_e^2}{k^2 V_{Te}^2(\omega^2 - l^2\Omega_e^2)} + \frac{1 - A_0(k_\perp^2\rho_e^2)}{k^2 r_{De}^2}. \tag{A3}$$

For the frequency spectrum of the electron Bernstein modes from (A3) we obtain

$$\omega^{(l)} = l\,|\Omega_e|\left(1 + \frac{I_l(k^2\rho_e^2)\exp(-k^2\rho_e^2)}{1 + k^2 r_{De}^2 - A_0(k_\perp^2\rho_e^2)}\right). \tag{A4}$$

In the long-wavelength region ($k^2\rho_e^2 \ll 1, k^2 r_{De}^2 \ll 1$), taking into account that $I_l(x) \sim x^l/2^l l!$, $x \ll 1$, we have

$$\omega^{(l)} = l\,|\Omega_e|\left(1 + \frac{(k^2\rho_e^2)}{2^l l!}\frac{(1 - k^2\rho_e^2)}{k^2 r_{De}^2}\right), \tag{A5}$$

and in the short-wavelength region, taking into account that $I_l(x) \sim e^x(\pi x)^{-1/2}$, $x \gg 1$,

$$\omega^{(l)} = l\,|\Omega_e|\left[1 + (1/\sqrt{\pi}k^3\rho_e r_{De}^2)\right]. \tag{A6}$$

From (A2) it is evident that the EBM ($k_z = 0$) are purely collisionally damped. The linear collisional damping rate is given by (see also Ref. 16, p. 93)

$$\gamma_{\mathrm{coll}}^{(l)} = \frac{\Omega_e^2\omega_{pe}^2\nu_{ei}k^2 r_{De}^2(l^2+1)A_l(k_\perp^2\rho_e^2)}{[\phi(l)]^2[1 + k^2 r_{De}^2 - A_0(k_\perp^2\rho_e^2)]^2}. \tag{A7}$$

The function $\phi(l)$ is defined by

$$\phi(l) = \omega_0^2 - \Omega_e^2 = (l+1)\Omega_e\left(\Omega_e(l-1) + l\Omega_e\frac{I_l(k^2\rho_e^2)}{1 + k^2 r_{De}^2 - A_0(k_\perp^2\rho_e^2)}\exp(-k_\perp^2\rho_e^2)\right). \tag{A8}$$

In (A8), $\omega_0 \sim \omega^{(l)}$ where $\omega^{(l)}$ is given by (A4). In the case of quasiperpendicular propagation $k_z/k > (m_e/m_i)^{1/2}$, the imaginary part of $\Gamma_+(x)$ is nonvanishing and, consequently, EC modes are Landau- and electron-cyclotron damped (for details see Ref. 19, pp. 267–288).

Along with the above considered modes propagating perpendicular and quasiperpendicular, obliquely propagating EC waves also exist in strongly magnetized plasmas ($\Omega_e > \omega_{pe}$). The corresponding dielectric permittivity and frequency spectrum [in (A1), $k^2\rho_e^2 \ll 1$ and $(\omega - l\Omega_\alpha)/|k_z|V_{Te} \gg 1$] are

$$\mathrm{Re}\,\epsilon(\omega, \mathbf{k}) = 1 - (\omega_{pe}^2/\omega^2 - \Omega_e^2)\sin^2\theta, \tag{A9}$$

$$\omega = \Omega_e\left[1 + \tfrac{1}{2}(\omega_{pe}/\Omega_e)^2\sin^2\theta\right]. \tag{A10}$$

In (A9) and (A10), θ is the angle between the wave vector $\mathbf{k}$ and $\mathbf{B}_0$. The excitation of this mode is very effective by the O-driver pump and the process can take place in the EC resonance layer in the case of axial launching from the high-field side of EBT [see Fig. 1, cases (b) and (c)].

From (A1), neglecting the ion response in the case where $\Omega_e < \omega < \omega_{\mathrm{UH}}(\Omega_e > \omega_{pe})$ and $(\omega - l\Omega_e)/|k_z|V_{Te} \gg 1 (n = 0, 1, \ldots)$, we have dielectric permittivity for upper-hybrid waves:

$$\mathrm{Re}\,\epsilon_{\mathrm{UH}} = 1 - A_0(k_\perp^2\rho_e^2)\frac{(k_z V_{Te})^2}{k^2 r_{De}^2\omega^2} - A_1(k_\perp^2\rho_e^2)\frac{2\Omega_e^2}{k^2 r_{De}^2(\omega^2 - \Omega_e^2)}, \tag{A11}$$

$$\mathrm{Im}\,\epsilon_{\mathrm{UH}} = -\gamma_{\mathrm{UH}}^{\mathrm{noncoll}}\left(\frac{\partial\,\mathrm{Re}\,\epsilon_{\mathrm{UH}}}{\partial\omega}\right)_{\omega=\omega_{\mathrm{UH}}} = \sqrt{\pi/2}\,\frac{\omega}{(kr_{De})^2(k_z V_{Te})} \times \sum_{l=0,1} A_l(k_\perp^2\rho_e^2)\exp\left(-\frac{(\omega - l\Omega_e)^2}{2(k_z V_{Te})^2}\right). \tag{A12}$$

In the long-wavelength region (this case is considered in Sec. IV) from (A11) and (A12), a known result for the cold upper-hybrid waves[18,19] could be obtained.

In the frequency range $\omega \sim n\Omega_i$, $n = 1, 2, \ldots$, and for EBT plasma, $\Omega_e \gtrsim \omega_{pe}$, $T_e \sim 20T_i$, using (A1) for the linear ion susceptibility we have $[(\omega - n\Omega_i)/|k_z|V_{Ti} \gg 1$, $n = 0, \pm 1, \pm 2, \ldots$, $\mathrm{Re}\,\Gamma_+(x) \sim 1 + 1/x^2]$:

$$\mathrm{Re}\,\chi_i(\omega, \mathbf{k}) = \frac{1}{k^2 r_{De}^2}\left(\frac{T_e}{T_i}\right)\left(1 - A_0(k_\perp^2\rho_i^2) - \sum_{n=1}^{\infty}\frac{2n^2 A_n\Omega_i^2}{\omega^2 - n^2\Omega_i^2} - \sum_{n=-\infty}^{+\infty}\frac{\omega k_z^2 V_{Ti}^2 A_n}{(\omega - n\Omega_i)^3}\right). \tag{A13}$$

For the electron susceptibility, if $\omega/|k_z|V_{Te} > 1$ and $|(\omega - n\Omega_e)|/k_z V_{Te} \sim \omega/k_z V_{Te}\Omega_e/\Omega_i \gg 1$, we have

$$\mathrm{Re}\,\chi_e(\omega, \mathbf{k}) = \frac{1}{k^2 r_{De}^2}\left(1 - A_0(k_\perp^2\rho_e^2) - A_0(k_\perp^2\rho_e^2)\frac{k_z^2 V_{Te}^2}{\omega^2} - \sum_{n=1}^{\infty}\frac{2n^2\Omega_e^2 A_n}{\omega^2 - n^2\Omega_e^2}\right). \tag{A14}$$

If, however, $\omega/|k_z|V_{Te} \ll 1$ and $|\omega - n\Omega_e|/|k_z| \times V_{Te} < 1$, then $\mathrm{Re}\,\Gamma_+(x) \sim x^2$, and consequently

$$\mathrm{Re}\,\chi_e(\omega, \mathbf{k}) = \frac{1}{k^2 r_{De}^2}\left(1 - A_0(k_\perp^2\rho_e^2)\frac{\omega^2}{k_z^2 V_{Te}^2} - \sum_{n=1}^{\infty}\frac{2A_n n^2\Omega_i^2}{k_z^2 V_{Te}^2}\right). \tag{A15}$$

For smaller k_z, with $\omega/|k_z|V_{Te} < 1$ and $|\omega - n\Omega_e|/|k_z|V_{Te} > 1$, we have

$$\mathrm{Re}\,\chi_e(\omega, \mathbf{k}) = \frac{1}{k^2 r_{De}^2}\left[1 - A_0(k_\perp^2\rho_e^2)\frac{\omega^2}{k_z^2 V_{Te}^2} - \sum_{n=1}^{\infty}\frac{2n^2\Omega_e^2 A_n}{\omega^2 - n^2\Omega_e^2}\left(1 + \frac{k_z^2 V_{Te}^2}{(\omega - n\Omega_e)^2}\right)\right]. \tag{A16}$$

The modes with linear susceptibilities given by (A13) and (A14) are called ion-Bernstein modes, and those with electron susceptibilities given by (A15) or (A16) are called ion-cyclotron waves. For the frequency spectrum of an ion-Bernstein mode we obtain

$$\omega = n\Omega_i\left(1 + \frac{T_e}{T_i}\frac{A_n(k^2\rho_i^2)}{1 + k^2 r_{De}^2 - A_0(k^2\rho_e^2) + (T_e/T_i)\,[1 - A_0(k^2\rho_i^2)]}\right), \tag{A17}$$

and for ion-cyclotron waves,

$$\omega = n\Omega_i\left(1 + \frac{T_e}{T_i}\frac{A_n(k^2\rho_i^2)}{1 + k^2 r_{De}^2 + (T_e/T_i)\,[1 - A_0(k^2\rho_i^2)]}\right). \tag{A18}$$

Ion-Bernstein modes for perpendicular propagation ($k_z = 0$) have pure collisional linear dissipation with linear damping rates (see also Ref. 16):

$$\gamma_{IB}^{coll} = \frac{56}{5n!2^n}\frac{n^2\Omega_i^4}{\omega_{pi}^4}\nu_{ii}(k^2\rho_i^2)^{2n+4}, \quad k^2\rho_i^2 \ll 1, \tag{A19}$$

$$\gamma_{IB}^{coll} = (3\sqrt{2}/8)(\pi + 1)(n^2\Omega_i^4/\omega_{pi}^4)\nu_{ii}(k\rho_i)^4, \quad k^2\rho_i^2 \gg 1. \tag{A20}$$

The case of pure collisionally damped IB modes is idealistic because complex magnetic field geometry in EBT will always lead to finite k_z. Accordingly, the modes will also be noncollisionally damped. Dominant linear dissipation is caused by the electron and ion Landau dampings ($\omega/k_z V_{Te} > 1$, $\omega/k_z V_{Ti} > 1$) and also the ion-cyclotron ($\omega - n\Omega_i)/|k_z| \times V_{Ti} > 1$, $n = 1, 2, \ldots$) dampings. In this case $\mathrm{Im}\,\Gamma_+(x) = -\sqrt{\pi/2}\exp(-x^2)$, and the linear damping rate has the form ($\omega \sim n\Omega_i$)

$$\gamma = -\sqrt{\frac{\pi}{2}}\frac{(\omega - n\Omega_i)^2}{k_z V_{Ti} A_n(k^2\rho_i^2)}\left[\left(\frac{T_i}{T_e}\right)^{3/2}\left(\frac{m_e}{m_i}\right)^{1/2} + \sum_{m=0,n} A_m(k^2\rho_i^2)\exp\left(-\frac{(\omega - n\Omega_i)^2}{2k_z^2 V_{Ti}^2}\right)\right]. \tag{A21}$$

For $k_z \to 0$, electron Landau damping becomes the dominant noncollisional dissipation mechanism.

[1] R. A. Dandl, H. O. Eason, G. E. Guest, C. L. Hedrick, H. Ikegami, and D. B. Nelson, in *Proceedings of the 5th International Conference on Plasma Physics and Controlled Nuclear Fusion Research* (IAEA, Vienna, 1975), Vol. 2, p. 141.

[2] N. A. Krall, in *Proceedings of the 2nd Hot Electron Ring Physics Workshop*, San Diego, California, 1981 (Oak Ridge National Laboratory, Oak Ridge, TN, 1982), Vol. 1, pp. 45–80.

[3] S. Hamasaki, H. H. Klein, N. A. Krall, J. B. McBride, and J. L. Sperling, Phys. Fluids **24**, 9 (1981).

[4] N. I. Zaytsev, T. B. Pankratova, M. I. Petelin, and V. A. Flyagin, Radio Eng. Electron Phys. **19**, 103 (1974); Y. Carmel, K. R. Chu, M. Read, A. K. Ganguly, D. Dialens, R. Seeley, J. S. Levine, and V. L. Granatstein, Phys. Rev. Lett. **50**, 112 (1983) (and references therein).

[5] V. V. Alikaev, G. A. Bobrovski, V. I. Poznyak, K. A. Razumova, V. V. Sanikov, Y. A. Sokolov, and A. A. Shmarin, Fiz. Plazmy **2**, 390 (1976) [Sov. J. Plasma Phys. **2**, 212 (1976)]; F. S. McDermott, G. Bekefi, K. E. Hackett, J. S. Levine, and M. Porkolab, Phys. Fluids **25**, 1488 (1982).

[6] T. M. Antonsen and W. M. Manheimer, Phys. Fluids **21**, 12 (1978); M. Bornatici and F. Engelman, Radio Sci. **14**, 309 (1979); R. A. Cairns and C. N. Lashmore-Davies, Phys. Fluids **26**, 1268 (1983); K. R. Chu and B. Hui, *ibid.* **26**, 69 (1983).

[7] M. S. Ioffe, B. I. Kanaev, V. P. Pastukhov, and E. E. Yushmanov, Zh. Eksp. Teor. Fiz. **67**, 2145 (1974).

[8] V. Stefan and N. A. Krall, Phys. Rev. Lett. **52**, 41 (1984).

[9] P. J. Catto, R. D. Hazeltine, S. Hamasaki, H. H. Klein, N. A. Krall, J. B. McBride, J. L. Sperling, C. L. Hedrick, D. B. Batchelor, L. E. Deleanu, R. C. Goldfinger, E. F. Jaeger, D. B. Nelson, D. A. Spong, J. T. Tolliver, N. A. Uckan, J. W. Van Dam, Y. C. Lee, and M. N. Rosenbluth, in *Plasma Physics and Controlled Nuclear Fusion Research*, 1980 (IAEA, Vienna, 1981), Vol. I, p. 821.

[10] V. Stefan and N. A. Krall, Bull. Am. Phys. Soc. **28**, 1177 (1983).

[11] R. C. Goldfinger, A. H. Kritz, and D. B. Batchelor, Nucl. Fusion **23**, 225 (1983).

[12] R. J. Colchin, T. Uckan, F. W. Baity, L. A. Berry, F. M. Bieniosek, L. Bighel, W. A. Davis, E. Dullni, H. O. Eason, J. C. Glowienka, G. A. Hallock, G. R. Haste, D. L. Hillis, A. Komori, T. L. Owens, R. K. Richards, L. Solenstein, T. L. White, and J. B. Wilgen, Plasma Phys. **25**, 597 (1983).

[13] N. A. Uckan and EBT Group, Plasma Phys. **25**, 129 (1983).

[14] J. B. McBride, N. A. Uckan, and R. J. Kashuba, Nucl. Technol. Fusion **4**, 497 (1983).

[15] M. Porkolab and R. P. H. Chang, Rev. Modern Phys. **50**, 745 (October 1978).

[16] V. P. Silin, *Parametric Action of High Power Radiation on Plasmas* (Nauka, Moscow, 1973), Chap. III, in Russian.

[17] P. K. Kaw, W. L. Kruer, C. S. Liu, and K. Nishikawa, in *Advances in Plasma Physics*, edited by A. Simon and W. B. Thomson (Interscience, New York, 1976), Vol. 6.

[18] N. A. Krall and A. W. Trivelpiece, *Principles of Plasma Physics* (McGraw-Hill, New York, 1973).

[19] A. I. Akhiezer, I. A. Akhiezer, R. V. Polovin, A. G. Sitenko and K. N. Stepanov, *Plasma Electrodynamics* (Pergamon, Oxford, 1975), Vol. 1.

[20] M. Porkolab, Phys. Fluids **17**, 1932 (1974); **20**, 2058 (1977).

[21] A. Bers, in *Handbook on Plasma Physics*, edited by A. A. Galeev and R. N. Sudan (North-Holland, Amsterdam, 1983), Vol. 1, Chap. 3.2.

[22] M. N. Rosenbluth, Phys. Rev. Lett. **29**, 565 (1972); A. A. Galeev, G. Laval, T. O'Neil, M. Rosenbluth, and R. Z. Sagdeev, Zh. Eksp. Teor. Fiz. Pis'ma **17**, 48 (1973) [Sov. Phys. JETP Lett. **17**, 35 (1973)].

[23] V. P. Silin and A. N. Starodub, Fiz. Plazmy **3**, 280 (1977) [Sov. J. Plasma Phys. **3**, 156 (1977)]; V. P. Silin and A. N. Starodub, Zh. Eksp. Teor. Fiz. **66**, 176 (1974) [Sov. Phys. JETP **39**, 82 (1974)].

[24] V. Stefan, Phys. Lett. **A32**, 8 (1981).

[25] V. Stefan and A. Bers, Phys. Fluids **27**, 175 (1984).

[26] J. McBride, Phys. Fluids **27**, 324 (1984); N. A. Krall and J. McBride, Phys. Fluids **28**, 2022 (1985).

[27] V. V. Pustovalov and V. P. Silin, Teor. Plazmy Tr. Fian **61**, 225 (1972), also available in English; *Theory of Plasmas, Proceedings of the Lebedev Physics Institute* (Consultants Bureau, New York, 1975), Vol. 61.

[28] B. B. Kadomtsev, *Plasma Turbulence* (Academic, New York, 1965), p. 31.

[29] V. Yu. Bychenkov, V. P. Silin, and V. T. Tikhonchuk, Sov. Phys. JETP Lett. **26**, 197 (1977).

[30] L. V. Krupnova, V. Stefan, and V. T. Tikhonchuk, Frika Plazmy **7**, 1350 (1981) [Sov. Plasma Phys. **7**, 744 (1981)].

[31] A. A. Galeev, R. Z. Sagdeev, V. D. Shapiro, and V. I. Shevchenko, in *Interaction of Strong Electromagnetic Waves with Collisionfree Plasma* (Academy of Sciences of the USSR, Institute of Applied Physics, Gorky, 1980), pp. 6–49, in Russian.

[32] E. Villalon and A. Bers, Nucl. Fusion **20**, 243 (1980).

[33] R. L. Berger and L. Chen, Phys. Fluids **19**, 1392 (1976).

[34] L. Dupas, P. Grelot, F. Parlange, and J. Weisse, in *Proceedings of the Eighth International Conference on Plasma Physics and Controlled Nuclear Fusion Research*, Brussels, 1980 (IAEA, Vienna, 1981), Vol. II, p. 489.

[35] W. L. Kruer and E. J. Valeo, Phys. Fluids **16**, 675 (1973).

[36] A. Hasegawa and L. Chen, Phys. Fluids **18**, 1321 (1975).

[37] V. K. Tripathi and C. S. Liu, Phys. Fluids **25**, 1388 (1982); O. P. Sharma, V. K. Tripathi, and C. S. Liu, *ibid.* **25**, 1598 (1982); C. S. Liu, V. S. Chan, V. K. Tripathi, and V. Stefan, *ibid.* **27**, 1709 (1984).

[38] A. T. Lin, C-C. Lin, and J. M. Dawson, Phys. Fluids **25**, 565 (1982).

[39] T. H. Stix, Phys. Rev. Lett. **15**, 878 (1965).

[40] J. M. Kindel, H. Okuda, and J. M. Dawson, Phys. Rev. Lett. **29**, 995

(1972); R. L. Berger and F. W. Perkins, Phys. Fluids **19**, 406 (1976); V. K. Tripathi, C. Grebogi, and C. S. Liu, *ibid.* **20**, 1525 (1977).
[41]T. H. Stix, *The Theory of Plasma Waves* (McGraw-Hill, New York, 1962).
[42]F. Troyon and F. W. Perkins, Bull. Am. Phys. Soc. **19**, 735 (1974).
[43]M. N. Rosenbluth, Phys. Rev. Lett. **29**, 565 (1972).
[44]J. L. Sperling, Phys. Rev. A **25**, 2707 (1982).
[45]V. E. Golant, J. Tech. Phys. **41**, 2492 (1971) [Sov. Phys. Tech. Phys. **16**, 212 (1972)].
[46]N. T. Gladd and N. A. Krall, Phys. Fluids **25**, 1241 (1982).
[47]T. H. Stix, Nucl. Fusion **15**, 737 (1975).
[48]F. W. Perkins, Nucl. Fusion **17**, 1197 (1977).
[49]M. Fujiwara, T. Kamimura, M. Hosokawa, T. Shoji, H. Iguchi, H. Sanuki, M. Tanaka, M. Aizawa, K. Takasugi, F. Tsuboi, H. Tsuchidate, M. Matsunaga, K. Kadota, A. Tsushima, K. W. Whang, and H. Ikegami, in *Plasma Physics and Controlled Nuclear Fusion Research*, 1983 (IAEA, Vienna, 1983), Vol. II, p. 197.
[50]F. W. Baity and T. L. Owens, IEEE Trans. Plasma Sci. **PS-11**, 19 (1983).
[51]R. R. Weynants, Phys. Rev. Lett. **33** 78 (1974).
[52]J. Hosea, D. Boyd, N. Bretz, R. Chrien, S. Cohen, P. Colestock, S. Davis, D. Dimock, P. Efthimion, H. Eubank, R. Golston, L. Grisham, E. Hinnov, H. Hsuan, D. Hwang, F. Jobes, D. Johnson, R. Kaita, J. Lawson, E. Mazzucatto, D. McNeill, S. Medley, E. Meservey, D. Mueller, G. Schilling, J. Schivell, G. Schmidt, A. Sivo, F. Stauffer, W. Stodiek, J. Strachan, S. Suckewer, G. Tait, H. Thompson, and G. Zankl, in *Plasma Physics and Controlled Nuclear Fusion Research*, 1980 (IAEA, Vienna, 1981), Vol. II, p. 95.
[53]J. C. Glowienka, W. A. Davis, D. L. Hillis, T. Uckan, F. M. Bieniosek, and L. Solensten, in *Proceedings of the 2nd Hot Electron Ring Physics Workshop* (Oak Ridge National Laboratory, Oak Ridge, Tennessee, 1981), Vol. II, pp. 609–632.
[54]F. W. Chambers and A. Bers, Phys. Fluids **20**, 466 (1977).
[55]V. L. Ginzburg and A. A. Rukhadze, *Waves in Magnetoactive Plasma* (Nauka, Moscow, 1975) pp. 101–102, in Russian.
[56]B. D. Fried and S. Conte, *Plasma Dispersion Function* (Academic, New York, 1961).